



# Global downscaled projections for climate impacts research (GDPCIR): preserving extremes for modeling future climate impacts

Diana R. Gergel<sup>1</sup>, Steven B. Malevich<sup>2</sup>, Kelly E. McCusker<sup>2</sup>, Emile Tenezakis<sup>2</sup>, Michael T. Delgado<sup>2</sup>, Meredith Fish<sup>3</sup>, and Robert Kopp<sup>3</sup>

<sup>1</sup>BlackRock, 601 Union Street, Seattle, WA 98101 USA

<sup>2</sup>Rhodium Group, 5 Columbus Circle, New York, NY 10019 USA

<sup>3</sup>Department of Earth and Planetary Sciences and Rutgers Institute of Earth, Ocean and Atmospheric Sciences, Rutgers University, 610 Taylor Road, Piscataway, NJ 08854 USA

**Correspondence:** Diana R. Gergel (dgergel@gmail.com)

## Abstract.

Global climate models are important tools for understanding the climate system and how it is projected to evolve under scenario-driven emissions pathways. Their output is widely used in climate impacts research for modeling the current and future effects of climate change. However, climate model output remains coarse in relation to the high-resolution climate data needed for climate impacts studies, and it also exhibits biases relative to observational data. Treatment of the distribution tails is a key challenge in existing downscaled climate datasets available at a global scale; many of these datasets used quantile mapping techniques that were known to dampen or amplify trends in the tails. In this study, we apply the trend-preserving Quantile Delta Mapping (QDM) bias-adjustment method (Cannon et al., 2015) and develop a new downscaling method called the Quantile-Preserving Localized-Analog Downscaling (QPLAD) method that also preserves trends in the distribution tails. Both methods are integrated into a transparent and reproducible software pipeline, which we apply to global, daily model output for surface variables (maximum and minimum temperature and total precipitation) from the Coupled Model Intercomparison Project Phase 6 (CMIP6) experiments (O'Neill et al., 2016) for the historical experiment and four future emissions scenarios ranging from aggressive mitigation to no mitigation: SSP1-2.6, SSP2-4.5, SSP3-7.0, and SSP5-8.5 (Riahi et al., 2017). We use European Centre for Medium-Range Weather Forecasts (ECMWF) ERA5 (Hersbach et al., 2018) temperature and precipitation reanalysis data as the reference dataset over the Sixth Intergovernmental Panel on Climate Change (IPCC) Assessment Report (AR6) reference period, 1995–2014. We produce bias-adjusted and downscaled data over the historical period (1950–2014) and for four emissions pathways (2015–2100) for 25 models in total. The output dataset of this study is the Global Downscaled Projections for Climate Impacts Research (GDPCIR), a global, daily, 0.25° horizontal-resolution product which is publicly hosted on Microsoft AI for Earth's Planetary Computer (<https://planetarycomputer.microsoft.com/dataset/group/cil-gdpcir/>).



## 20 1 Introduction

Global climate models (GCMs) are essential for studying the climate system and how it will evolve in the future. Simulations from the Coupled Model Intercomparison Project (CMIP) experiments are widely used in climate impact studies, exploring human health (e.g., Carleton et al., 2022), energy (e.g., Rode et al., 2021), labor productivity (e.g., Parsons et al., 2022), agriculture crop yields (e.g., Müller et al., 2021), and the impacts of climate change on GDP losses globally (e.g., Warren et al., 2021). However, despite progress in climate modeling, GCM simulations often exhibit systematic error (bias) relative to observations (François et al., 2020) due to coarse spatiotemporal resolution, simplified physics, thermodynamic schemes, and incomplete and/or poorly understood representation of climate system processes (Sillmann et al., 2013). GCM simulations, relative to historical observations, can have large errors in their means and variance, and even larger biases in extreme values (Cannon et al., 2015). All of these biases are challenging to impacts studies examining the future evolution of local climate impacts. This challenge is magnified when trying to understand how a particular climate extreme will affect a given outcome, for example, how extreme temperatures will affect mortality rates in a location expected to experience large temperature increases throughout the twenty-first century. To explore these questions, it is necessary to have high-resolution climate projections for multiple emissions pathways with a statistical distribution consistent with historical observations.

To fill this need, statistical bias adjustment (BA) and downscaling methods are used to adjust biases and add high-resolution spatial information to the coarse resolution of GCM simulations. BA methods adjust the difference in statistical properties between model simulations and observations. In this context, downscaling is the process of moving from the coarse resolution of the GCM to the high-resolution local information needed to use as inputs for impacts models. The majority of statistical BA methods adjust the GCM simulation distribution by operating on the mean, variance, higher moments, or quantiles (François et al., 2020). These methods, particularly traditional quantile mapping ones, are known to affect trends in extreme quantiles differently than trends in the mean, thus degrading results at the distribution tails (Maurer and Pierce, 2014; Lehner et al., 2021; Holthuijzen et al., 2022). Standard quantile mapping (QM) methods were used to create the popular NASA Earth Exchange (NEX) Global Daily Downscaled Projections (GDDP) global daily CMIP5 dataset (Thrasher et al., 2012), which uses the Bias Correction and Spatial Disaggregation (BCSD) QM approach. However, the method differentially affects trends in extreme quantiles, degrading the tails of the distribution. BCSD for example adjusts GCM simulations to have the same cumulative distribution function (CDF) as the reference dataset (for each day of the year) and then imposes a 9-year running monthly mean trend from the GCM on the adjusted-day value (Thrasher et al., 2012). This does not preserve trends in the tails of the distribution because the GCM trend imposed is the mean-monthly trend. Maurer and Pierce (2014) found that QM modifications of projected trends in seasonal mean model precipitation could be as large as the actual GCM-projected changes.

Downscaling faces similar challenges to bias-adjustment methods (Cannon et al., 2020). Downscaling in BCSD, for example, dampens trends in the tails of the higher-resolution gridcells because the method involves bilinearly interpolating scaling factors computed as the difference (or ratio) of GCM to reanalysis climatologies on a per-pixel multi-decade basis. Because of these challenges, many studies in the impacts literature stop short of downscaling (Maraun, 2016). Others, such as Lange (2019), combine trend-preserving bias adjustment with statistical downscaling, but the final resolution of the downscaled data remains



relatively coarse ( $0.5^\circ$ ). This effect is undesirable for climate impacts modeling because it dampens or amplifies trends in the tails, which are crucial to understanding how climate extremes and their associated impacts will evolve for various emissions pathways (Sanabria et al., 2022; Lanzante et al., 2020). Returning to the mortality impacts example, it is not sufficient to project the future mean rise in temperature at a given location. Trends for the hottest days must be preserved to understand and project mortality impacts.

Several CMIP6 downscaling datasets produced in the past several years have attempted to address these issues, but they have either been limited in geographic scope (e.g., Supharatid et al., 2022), global but at a coarse spatial resolution (e.g., Xu et al., 2021), or global but preserving only mean trends (e.g., Thrasher et al., 2021). Moreover, Jupiter Intelligence (<https://jupiterintel.com/>), a climate risk-focused company in the private sector, has made a CMIP6 dataset available for commercial applications. Unfortunately, its methods are neither published nor transparent and the dataset is not publicly available (Hacker, 2021). The Intersectoral Impact Model Intercomparison Project (ISIMIP) downscaled dataset (Lange, 2019) uses trend-preserving bias adjustment and downscaling approaches on daily data at a global scale, but it is only available for a limited number of GCMs, at a  $0.5^\circ$  spatial resolution. In the past year, several downscaled datasets for CMIP6 at a higher spatial resolution have been released. NASA updated the NASA-NEX dataset using CMIP6 projections and released the new dataset in early 2022 (Thrasher et al., 2022) but still relies on the BCSD method. Additionally, the updated NASA-NEX GDDP dataset still relies on the Global Meteorological Forcing Dataset (GMFD) (Sheffield et al., 2006), a reanalysis dataset that now dated and no longer widely used in bias adjustment and downscaling (Hassler and Lauer, 2021). CarbonPlan, a not-for-profit organization focused on climate and carbon capture research, has also released a global downscaled CMIP6 dataset using four distinct statistical downscaling methods (<https://docs.carbonplan.org/cmip6-downscaling>). While this is an important contribution to method transparency and comparison, the monthly resolution of the dataset is prohibitively coarse for many impacts modeling applications and the dataset is only available for a subset of six GCMs.

To ameliorate these challenges for impacts modelers, this study uses statistical bias adjustment and downscaling methods that explicitly preserve relative changes in GCM simulation quantiles (Cannon et al., 2015). We use the quantile delta mapping (QDM) method (Cannon et al., 2015) for bias adjustment. For downscaling, we introduce the Quantile-Preserving Localized-Analog Downscaling (QPLAD) method, a novel statistical downscaling algorithm that applies a local analog-mapping approach to preserve quantile trends at the fine resolution. We have made the methods and code transparent and reproducible. The dataset described herein, titled Global Downscaled Projections for Climate Impacts Research (GDPCIR), is, to our knowledge, the most comprehensive and high-resolution dataset that exists for CMIP6 that preserves quantile trends. The preservation of quantile trends makes the dataset better suited for impacts modeling than other downscaled CMIP6 datasets since high and low tail trends are not dampened or amplified by only accounting for mean projected changes.

The remainder of the paper is structured as follows. In Section 2, we describe the climate simulations and reference dataset. In Section 3, we describe the QDM-QPLAD bias adjustment and downscaling methods. Section 4 describes our downscaling pipeline and efforts to make our pipeline implementation on commercial cloud computing platforms transparent and reproducible. In Section 5, we explore trends and extremes in the dataset at the global, city, and “admin1” (country) levels. In the final section, we detail applications for econometric research for climate risk and other impacts modeling areas.



## 2 Climate data

### 90 2.1 Simulation data

We used the CMIP6 GCM experiments (Eyring et al., 2016; O'Neill et al., 2016) as simulation data. We obtained the data from the Google Cloud CMIP6 collection (<https://pangeo-data.github.io/pangeo-cmip6-cloud/>). This contains a subset of CMIP6 output migrated from the Earth System Grid Federation (ESGF) as part of a collaboration between the Pangeo Consortium (<https://pangeo.io/>), Lamont-Doherty Earth Observatory (LDEO) and Google Cloud. The migration to Google Cloud included data from NetCDF format (<https://www.unidata.ucar.edu/software/netcdf/>) to the cloud-optimized Zarr store format (<https://zarr.readthedocs.io/en/stable/api/storage.html>), and standardizing across dimensions, coordinates, and grids to ensure that model output would be analysis-ready and cloud-hosted for streamlined use in scientific analysis Abernathy et al. (2021). CMIP6 output available through the ESGF but not in the CMIP6 Google Cloud collection was excluded because it was not analysis-ready and cloud-optimized, and as such, could not run through our cloud-based downscaling pipeline.

100

In addition to the last 65 years of the historical CMIP experiment, we included four 21st century ScenarioMIP experiments so as to span a range of possible future climate trajectories. These trajectories are defined by a combination of Shared Socioeconomic Pathways (SSPs) and Representative Concentration Pathways (RCPs): SSP1-2.6, SSP2-4.5, SSP3-7.0, and SSP5-8.5 (Riahi et al., 2017). We did not include simulations that have output populated with NaNs for some years or did not have complete spatiotemporal coverage. For example, the Hammoz-Consortium model is not included because its temperature output available through the Google Cloud CMIP6 collection did not extend past 2055. We also do not include the Community Earth System Model from the National Center for Atmospheric Research (NCAR) because there was no historical daily surface variable output available through NCAR for the historical experiment. We perform bias adjustment and downscaling on a subset of the historical CMIP experiment (1950–2014) and ScenarioMIP scenarios (2015–2100) with a historical training period from 1995 to 2014, consistent with the IPCC AR6 reference period. The full dataset includes 25 GCMs (Table 1), with downscaled output for all four SSPs available for the majority of those GCMs. If an SSP is missing for a given GCM, that indicates that it was either not available in the CMIP6 Google Cloud collection or we found issues with the data available. If a GCM from a modeling center that participated in the CMIP6 experiments is missing, that indicates that the GCM did not have daily surface variable output available for maximum and minimum temperature and surface precipitation in the CMIP6 Google Cloud collection as of 15 November 2021, or the output that was available contained data issues as discussed above.

115

We standardize calendars across all GCMs included in the dataset by converting them to a 365-day (e.g., “no-leap”) calendar. Leap days are removed for GCMs with 366-day calendars. For the two GCMs on 360-day calendars, we follow the method in Pierce et al. (2014). Five days per year are chosen randomly to add to the calendar, each in a given fifth of the year. Feb. 29th is always missing. For each of the days that are added, a day value is produced by averaging the adjacent days. For example, if Feb. 16th is the day added in the first fifth of the year for a given year, it will be the average of Feb. 15th and Feb. 17th.

120



Choosing a random day in a fifth of the year versus the same five days every year mitigates overall undesired effects on the statistics of particular days of the year or annual cycle statistics when converting from a 360-day to 365-day calendar.

<b>GCM</b>	<b>Institution</b>	<b>SSPs</b>
BCC-CSM2-MR	Beijing Climate Center, Beijing, China	SSP1-2.6, SSP2-4.5, SSP3-7.0, SSP5-8.5
FGOALS-g3	Chinese Academy of Sciences, Beijing, China	SSP1-2.6, SSP2-4.5, SSP3-7.0, SSP5-8.5
CanESM5	Canadian Centre for Climate Modelling and Analysis, Victoria, BC	SSP1-2.6, SSP2-4.5, SSP3-7.0, SSP5-8.5
CMCC-CM2-SR5	Fondazione Centro Euro-Mediterraneo sui Cambiamenti Climatici, Lecce, Italy	SSP1-2.6, SSP2-4.5, SSP3-7.0, SSP5-8.5
CMCC-ESM2	Fondazione Centro Euro-Mediterraneo sui Cambiamenti Climatici, Lecce, Italy	SSP1-2.6, SSP2-4.5, SSP3-7.0, SSP5-8.5
ACCESS-ESM1-5	Commonwealth Scientific and Industrial Research Organisation, Aspendale, Victoria, Australia	SSP1-2.6, SSP2-4.5, SSP3-7.0
ACCESS-CM2	Commonwealth Scientific and Industrial Research Organisation, Aspendale, Victoria, Australia	SSP2-4.5, SSP3-7.0
MPI-ESM1-2-HR	Deutscher Wetterdienst, Offenbach am Main, Germany	SSP1-2.6, SSP5-8.5
MPI-ESM1-2-LR	Max Planck Institute for Meteorology, Hamburg, Germany	SSP1-2.6, SSP2-4.5, SSP3-7.0, SSP5-8.5
EC-Earth3	EC-Earth-Consortium	SSP1-2.6, SSP2-4.5, SSP3-7.0, SSP5-8.5
EC-Earth3-AerChem	EC-Earth-Consortium	SSP3-7.0
EC-Earth3-CC	EC-Earth-Consortium	SSP2-4.5, SSP5-8.5
EC-Earth3-Veg	EC-Earth-Consortium	SSP1-2.6, SSP2-4.5, SSP3-7.0, SSP5-8.5
EC-Earth3-Veg-LR	EC-Earth-Consortium	SSP1-2.6, SSP2-4.5, SSP3-7.0, SSP5-8.5
INM-CM4-8	Russian Academy of Science, Moscow, Russia	SSP1-2.6, SSP2-4.5, SSP3-7.0, SSP5-8.5



INM-CM5-0	Russian Academy of Science, Moscow, Russia	SSP1-2.6, SSP2-4.5, SSP3-7.0, SSP5-8.5
MIROC-ES2L	Japan Agency for Marine-Earth Science and Technology, Kanagawa, Japan	SSP1-2.6, SSP2-4.5, SSP3-7.0, SSP5-8.5
MIROC6	Japan Agency for Marine-Earth Science and Technology, Kanagawa, Japan	SSP1-2.6, SSP2-4.5, SSP3-7.0, SSP5-8.5
HadGEM3-GC31-LL	Met Office Hadley Centre, Exeter, Devon, United Kingdom	SSP1-2.6, SSP2-4.5, SSP5-8.5
UKESM1-0-LL	Met Office Hadley Centre, Exeter, Devon, United Kingdom	SSP1-2.6, SSP2-4.5, SSP3-7.0, SSP5-8.5
NorESM2-LM	NorESM Climate Modeling Consortium, Oslo, Norway	SSP1-2.6, SSP2-4.5, SSP3-7.0, SSP5-8.5
NorESM2-MM	NorESM Climate Modeling Consortium, Oslo, Norway	SSP1-2.6, SSP2-4.5, SSP3-7.0, SSP5-8.5
GFDL-CM4	NOAA Geophysical Fluid Dynamics Laboratory, Princeton, NJ, USA	SSP2-4.5, SSP5-8.5
GFDL-ESM4	NOAA Geophysical Fluid Dynamics Laboratory, Princeton, NJ, USA	SSP1-2.6, SSP2-4.5, SSP3-7.0, SSP5-8.5
NESM3	Nanjing University of Information Science and Technology, Nanjing, China	SSP1-2.6, SSP2-4.5, SSP5-8.5

Table 1: Full list of Coupled Model Intercomparison Project (CMIP6) models included in the GDPCIR dataset along with their corresponding institutions and the available SSPs for each model.

## 2.2 Reference data

125 We use the ECMWF Reanalysis v5 (ERA5) (Hersbach et al., 2018) as the historical reference dataset for bias adjustment and  
downscaling. ERA5 reanalysis data is produced and archived on a reduced Gaussian grid with a resolution of N320, meaning  
that there are 320 quasi-regularly spaced latitude points from pole to equator, at a 31 km (0.28°) resolution. We obtained  
global, hourly temperature and precipitation estimates from 1979 through 2018 on a regular (latitude-longitude) Gaussian grid  
at the same resolution to minimize the impact of interpolation from the Copernicus Data Service regridding, particularly on  
130 precipitation. We derive daily maximum and minimum temperatures by taking the daily maximum and minimum of the hourly  
values and total daily precipitation by taking the sum of hourly values. ERA5 hourly precipitation values represent cumulative  
precipitation during the preceding hour, thus cumulative daily precipitation for a given day is the sum of hourly values minus  
the first hour and including the first hour of the following day. We then subset the ERA5 daily surface variables to 1995–2014



to be consistent with the historical reference period used in Masson-Delmotte et al. (2021), finally, we remove leap days. We  
135 use the resulting 20-year ERA5 dataset as the historical reference data for bias adjustment and downscaling.

### 3 Methods

#### 3.1 Statistical bias adjustment with the QDM method

In this study, our goal was to emphasize downscaling and bias-adjustment methods that better preserve the extreme tails of  
distributions, but within the constraints of the level of method complexity that could be undertaken given the scale of this  
140 project. Though some multivariate statistical methods might have better preserved joint correlations between variables, such  
as Multivariate Bias adjustment (Cannon, 2018), the computational intensity of even running a univariate method at this scale  
precluded the choice of a multivariate method. Some studies have also found that multivariate methods may lead to degraded re-  
sults for one or more variables (e.g., temperature) that are being jointly bias-adjusted and/or downscaled, and also may perform  
poorly under projected climate change due to bias nonstationarity (Van de Velde et al., 2020; François et al., 2020). Choosing  
145 a method that would not degrade temperature projections was necessary given the role of temperature as a key driver of future  
climate impacts. With these constraints in mind, and after evaluating a number of statistical methods and their effects on the  
distribution tails, we chose the QDM method. The QDM statistical bias-adjustment method preserves changes in quantiles  
by applying simulated changes in the quantiles on top of the historical reference distribution (Cannon et al., 2015). Absolute  
changes or relative changes are preserved for additive or multiplicative variables, respectively. As a result, treatment of the  
150 tails is better than in standard quantile mapping as well as in empirical quantile mapping (EQM), detrended quantile map-  
ping (DQM), and various parametric and non-parametric variants of each (Qian and Chang, 2021). This rationale, combined  
with the QDM method being relatively computationally inexpensive compared to multivariate quantile mapping or machine  
learning-based methods, makes it a favorable method choice for a project of this scope and aim.

155 The QDM method adjusts the bias in projected values for a historical or future time period by first shifting the distribution  
to be consistent with the reference dataset and then imposing the relative GCM-projected trend, resulting in a bias-adjusted  
projection that has a distribution consistent with that of the reference dataset and also has a relative trend consistent with the  
source GCM, for a given quantile. In detail, following the notation in Cannon et al. (2015), let  $F_{m,p}[\cdot]$ ,  $F_{m,h}[\cdot]$  and  $F_{o,h}[\cdot]$   
denote, respectively, the CDF from model  $m$  in future period  $p$ , the CDF from model  $m$  in the historical period  $h$  and the  
160 CDF from the reference data  $o$  in the historical period  $h$ . Let  $x_{m,p}$  be a modeled future value at time  $t$  (for example, maximum  
temperature on 13 March 2025), and let  $x_{m,p}^*$  be the associated adjusted value for the same future date. In addition, let  $\tau_{m,p}$   
denote the non-exceedance probability associated with  $x_{m,p}$ , i.e  $\tau_{m,p} = F_{m,p}[x_{m,p}]$ .  $F^{-1}[\cdot]$  represents the inverse CDF. The  
adjusted value is defined as follows for an additive variable:

$$x_{m,p}^*(t) = x_{m,p}(t) + (F_{o,h}^{-1}[\tau_{m,p}(t)] - F_{m,h}^{-1}[\tau_{m,p}(t)]) \quad (1)$$



165 Rearranging the right-hand side shows that Equation 1 is equivalent to introducing the GCM-projected change at a given quantile ( $\tau_{m,p}$ ) on top of the reference data value at that quantile:

$$x_{m,p}^*(t) = \underbrace{F_{o,h}^{-1}[\tau_{m,p}(t)]}_{\text{reference value at model quantile}} + \underbrace{(x_{m,p}(t) - F_{m,h}^{-1}[\tau_{m,p}(t)])}_{\text{model trend in quantile}} \quad (2)$$

For a multiplicative variable such as precipitation, the right-hand side in equations (1) and (2) becomes multiplicative rather than additive, i.e., Equation 1 becomes  $x_{m,p}^* = x_{m,p} * F_{o,h}^{-1}[\tau_{m,p}]/F_{m,h}^{-1}[\tau_{m,p}]$ . This results in GCM projections that preserve each GCM's change in distribution shape (including extremes) while simultaneously making the training-period distribution consistent with the reference dataset.

### 3.2 Statistical trend-preserving downscaling with the QPLAD method

A key goal of downscaling for climate impacts is increasing spatial resolution in a way that both preserves climate trends and introduces realistic local climatology and variability. In observations, the climate signal at a coarser scale will always – by definition – represent a smoothed version of local climate trends. Similarly, high-resolution climate projections need to have a distribution that is consistent with locally observed climate. Downscaling may break consistency with the original GCM dynamics, but this is necessary to produce the spatial heterogeneity required for modeling climate impacts (Maraun and Widmann, 2018). Traditional downscaling methods typically work by introducing the climatological fine reference spatial pattern to the coarse resolution simulated data, as a difference or ratio between fine and coarse. This can have the effect of modifying trends and spatial patterns in the tails of the simulated distribution. To address this, we developed the QPLAD method. The QPLAD method uses the difference in empirical quantiles of the reference data — each quantile is a given day, or “analog” of the reference training period – at coarse and fine resolution to downscale the coarse resolution GCM simulations. The outcome is a downscaled dataset that preserves the changes in coarse GCM quantiles in time while also reflecting the within-coarse-grid cell spatial heterogeneity from the fine reference data. As a result, localized, extreme changes in the downscaled data are consistent with the GCM projections.

Formally, QPLAD involves computing and applying “adjustment factors” for each quantile in the reference data over the training period. First, an empirical CDF,  $F_{o,h,c}[\cdot]$ , of the reference data  $o$ , over the training period  $h$  at the relatively “coarse” resolution  $c$  at which bias adjustment was applied to GCMs. The method described here in the GDPCIR pipeline assumes that bias adjustment was performed at a coarser resolution than the target resolution for downscaling, but theoretically one could apply QPLAD to unadjusted GCM simulations as well. The number of empirical quantiles  $q$  is equal to the number of time steps in the training period  $n$  (e.g., a training period of 20 years with a 31-day rolling window has  $n = q = 20 * 31 = 651$ , since each empirical quantile corresponds to a day in the training period). Next, the reference data at “fine” resolution is sorted into the same order as the coarse resolution empirical CDF,  $B_{o,h,f}[\cdot]$ , where the set  $B$  represents the fine reference time steps (days) sorted the same as the coarse CDF  $F_{o,h,c}[\cdot]$  and  $f$  refers to the fine resolution. Adjustment factors are then calculated as the difference or ratio (for an additive or multiplicative variable, respectively) between the fine and coarse resolution values for





each historical analog day in the sorted data (i.e., for each empirical quantile). For an additive variable, adjustment factors  $af$  are as follows:

$$af(q_c) = B_{o,h,f}^{-1}(q_c) - F_{o,h,c}^{-1}(q_c) \quad (3)$$

for all coarse empirical quantiles  $q_c$ , where  $B^{-1}[\cdot]$  represents the fine reference values (rather than quantiles) in sorted order. Similar to QDM detailed above, the adjustment factors are applied to coarse resolution simulations by first determining the quantile of a given time step's value,  $F_{m,p,c}(x_{m,p,c}) = \tau_{m,p}$  where  $\tau_{m,p}$  is the non-exceedance probability associated with the value  $x_{m,p,c}$ . For an additive variable, the downscaled value for a given time step  $t$  in the projection simulation is defined as:

$$\tilde{x}_{m,p,f}(t) = x_{m,p,c}(t) + af_{q_c} \quad (4)$$

This results in high-resolution, downscaled projections where the subgrid cell heterogeneity from the original coarse resolution contains the more extreme days from the higher-resolution reference data. By definition, all of the target fine-resolution grid cells encompassed by the coarse-resolution grid cell will have downscaled values that average to the value for the coarse grid cell. In this way, “quantile-preserving” refers to maintaining the quantile information from the coarse-resolution day, and “localized” refers to the fine-resolution historical analogs located within a coarse-resolution grid cell. The method produces downscaled projections that add high-resolution information from the reference data training period and ensure that the fine-resolution spatial make-up of more extreme days from the coarse simulations are coherent and analogous to those found in the reference data. Thus, extreme days are also preserved in the downscaled projections in a relative sense (in a similar manner to QDM). Note that the QDM and QPLAD methods, which explicitly preserve changes in the quantiles, do not necessarily preserve model-projected changes in the mean due to using empirical CDFs, which is a non-parametric approach. Taking a parametric approach and using an analytical CDF would preserve changes in the mean, but would also impose a distribution to the CDFs. As Lehner et al. (2021) discuss, the question of whether to take a parametric or non-parametric approach in bias adjustment is an active area of research, but the non-parametric approach in the QDM and QPLAD methods is more common and generally preferred.

### 3.3 Wet day frequency adjustment

The discrete and continuous nature of the daily precipitation data needs to be addressed when applying bias adjustment and downscaling. Moreover, GCMs are known to have a “drizzle day” problem where the frequency of wet days with low precipitation in GCMs has a high positive bias relative to observations (Dai, 2006). To account for these issues, we apply a “pre” wet day frequency (WDF) adjustment to both reference and daily GCM data after regridding both datasets to the  $1^\circ$  bias adjustment grid and before bias adjusting. We apply a second “post” WDF adjustment after QPLAD downscaling.

Our approach is modified from Cannon et al. (2015). For daily reanalysis and GCM precipitation before bias adjustment, all values at the  $1^\circ$  grid that are less than a specified threshold are replaced by nonzero uniform random values less than the



threshold. Initially, we used the same threshold and nonzero uniform random values as Cannon et al. (2015). However, we found that in grid cells where the seasonality and magnitude of daily precipitation values differed by a large amount between model and reanalysis, using the Cannon et al. (2015) threshold ( $0.05 \text{ mm day}^{-1}$ ) and adjustment could result in those grid cells having bias-adjusted precipitation values that were not physically realistic for the season and geographic location. Thus we raised the threshold to  $1.0 \text{ mm day}^{-1}$  (similar to Hempel et al., 2013) and the lower bound of the uniform random distribution from 0 to  $0.5 \text{ mm day}^{-1}$ . After applying QPLAD downscaling, we then apply a “post” WDF adjustment where all downscaled daily precipitation values below  $1.0 \text{ mm day}^{-1}$  are replaced by  $0 \text{ mm day}^{-1}$ .

#### 4 Implementing the downscaling pipeline

In this section, we describe the pipeline we created for ingesting CMIP6 global, daily surface variable output from the CMIP6 Google Cloud collection, and applying statistical bias-adjustment and downscaling methods to produce a global, daily gridded dataset at a  $0.25^\circ$  horizontal resolution for four emissions pathways, 25 GCMs and three surface variables. The steps to produce the dataset are as follows and diagrammed in Figure 1: We first standardize the reference dataset and climate model output. We then apply a modified version of the QDM bias-adjustment method at the  $1^\circ$  grid. Next, we apply the QPLAD downscaling method to the bias-adjusted output in order to downscale the data to a  $0.25^\circ$  grid. For precipitation, we apply a wet day frequency adjustment both before bias adjusting and after downscaling. We apply additional post-processing for all surface variables after downscaling.

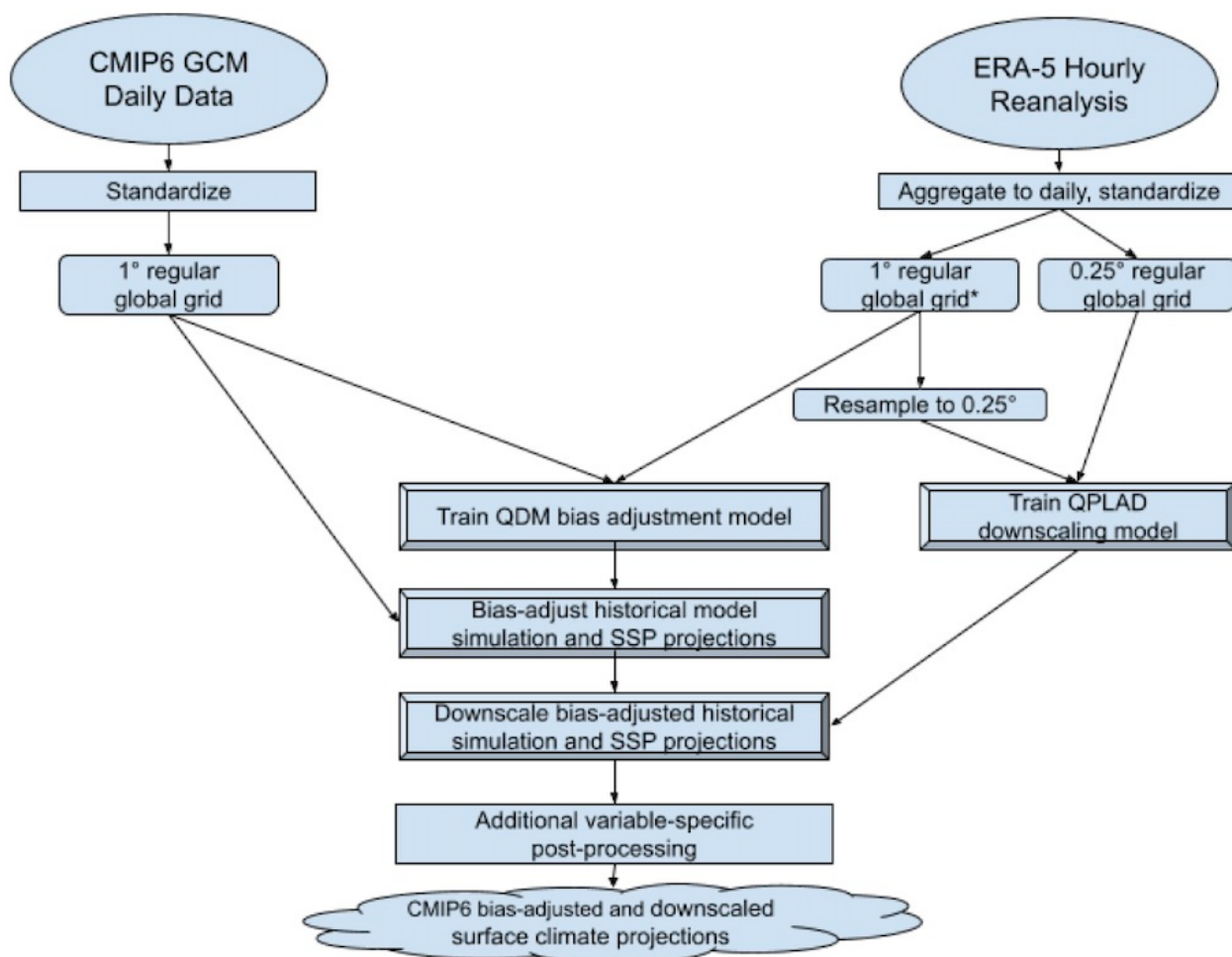


**Figure 1.** Diagram of CMIP6 bias adjustment and downscaling pipeline.

#### 245 4.1 Standardizing simulation and reference data

Although the modeling centers participating in the CMIP6 experiments follow Climate and Forecast (CF) conventions (<https://cfconventions.org/>), significant differences remain in how GCM output is archived. The native resolution of GCMs also varies considerably. For example, four EC-Earth Consortium models have a relatively high resolution (spectral grids approximately  $0.7^\circ \times 0.7^\circ$ ) and the CCCma CanESM5 GCM has a relatively low resolution ( $2.5^\circ \times 2.5^\circ$ ). Consequently, we begin  
250 by standardizing naming, dimensions, and coordinates for all models and removing leap days. Daily GCM outputs are regrid-  
ded from the models' native resolution to a regular  $1^\circ \times 1^\circ$  global lat-lon grid using the xESMF Python regridding package  
(<https://xesmf.readthedocs.io/>). We use the bilinear regridding method for maximum and minimum surface temperature and



first-order conservative area remapping for precipitation to conserve total precipitation between the native GCM grid and the  $1^\circ \times 1^\circ$  regular lat-lon grid.

255 The same standardization is applied to daily ERA5 reanalysis at the regular Gaussian, F320 grid. We prepare three versions of ERA5 that are used in the QDM-QPLAD method. For bias adjustment, ERA5 is regridded from the F320 grid to the  $1^\circ \times 1^\circ$  regular lat-lon grid using the regridding method described above. For downscaling, ERA5 is regridded from the F320 grid to the  $0.25^\circ \times 0.25^\circ$  regular lat-lon grid using the same regridding methods as in the GCM output ( $ERA5_{fine}$ ). Then, the  $1^\circ \times 1^\circ$  version of ERA5 used in bias adjustment is resampled (e.g., nearest-neighbor regridded) to the  $0.25^\circ \times 0.25^\circ$  regular lat-lon  
260 grid ( $ERA5_{coarse}$ ).

## 4.2 Implementation of QDM bias adjustment

We bias adjust GCM projections for each variable, GCM, experiment, pixel, year, and day at a  $1^\circ \times 1^\circ$  resolution using the xclim Python package QDM implementation (Logan et al., 2021). To do this, we first train QDM models for each pixel and day of the year using a rolling 31-day centered window ( $\pm 15$  days) on ERA5 and GCM historical data. For ERA5 data, we  
265 include the last 15 days from 1994 and the first 15 days from 2015 such that each day group contains 620 values (20 years  $\times$  31 days) for ERA5 reference data. For CMIP6 historical data, since the simulation ends in 2014, we do not include the additional 15 days from 2015, nor from 1994 for consistency. Each trained QDM model (per pixel / day of year) has 100 equally spaced quantiles in our implementation. We used an additive adjustment for maximum and minimum temperature and a multiplicative adjustment for precipitation. Each variable was bias-adjusted separately.

270 One pitfall with this approach is that minimum temperatures may be larger than maximum temperatures on the same day in some parts of the world with very low diurnal temperature ranges, such as at high latitudes (Thrasher et al., 2012). As a post-processing step, we swapped minimum and maximum temperatures for the small number of pixels and days when the minimum temperature exceeded the maximum temperature after downscaling. This post-processing is described further in Section 4.3.1. We initially tried to avoid this issue by adjusting the maximum temperature using an additive adjustment,  
275 separately adjusting the diurnal temperature range (DTR) using a multiplicative adjustment and then deriving the minimum temperature by subtracting DTR from the maximum temperature (following Agbazo and Grenier (2020)). However, we found that this led to unrealistically large DTR values in some parts of the globe, particularly at higher latitudes. Additionally, some raw GCM data had a small number of minimum temperatures greater than the corresponding maximum temperatures, more often in polar regions. Bias adjustment then inflated this undesirable behavior. Therefore, we bias-adjusted and downscaled  
280 maximum and minimum temperatures separately rather than bias-adjusting DTR.

We apply the trained QDM models to historical CMIP simulations and future GCM projections for each SSP on a per variable/GCM/pixel/year/day basis. For each year in the GCM data, we group daily data using a 21-year rolling window and a rolling 31-day window (as in the training step, with  $\pm 15$  days). For historical CMIP experiments, we concatenate the first eleven years (2015–2025) of the SSP3-7.0 projection period simulation so that the full historical dataset encompasses the years  
285 1950–2025. We use SSP3-7.0 to best simulate the current trajectory of emissions since 2015. If SSP3-7.0 output is not available for a given GCM, we then use SSP2-4.5. For the few models in which neither SSP3-7.0 nor SSP2-4.5 output is available, we



use SSP1-2.6. For each SSP, we concatenate the last eleven years (2004–2014) of the CMIP model simulation so that the full projection period dataset encompasses the years 2004–2100 for the rolling 21-year window. Historical GCM years 1950–1960 have fewer days in their rolling window, as do projection period years 2090–2100, with the exception of GCMs for which model output was available past 2100 in the CMIP6 Google Cloud collection at run-time. For the beginning (ends) of the time period, an additional 15 days from the previous (following) year is included such that each day group contains 651 values (21 years x 31 days). We use 100 equally-spaced quantiles as in the training step; adjustment factors for quantiles within the range [0.005, 0.995] are linearly interpolated from the neighboring quantiles and linear extrapolation is used to extend the range to 0 and 1 for accommodating the extreme tails.

### 295 4.3 Implementation of QPLAD downscaling

After applying QDM bias adjustment, we downscale GCM projections for each variable, model, experiment, pixel, year, and day at a  $0.25^\circ \times 0.25^\circ$  resolution, similar to our handling of QDM bias adjustment. To facilitate this, we implemented the QPLAD method in a forked version of the xclim Python package (Logan et al., 2021) in order to leverage the existing parallelization that we used for QDM, and we are in the process of adding the method to the package. Before downscaling, we resample the bias-adjusted projections from the  $1^\circ \times 1^\circ$  bias adjustment grid resolution to the  $0.25^\circ \times 0.25^\circ$  target resolution. For all variables, the method is consistent to ensure that each of the 16  $0.25^\circ$  gridcells contained within each  $1^\circ$  gridcell has the same value. Reanalysis data preparation for QPLAD is described in Section 3.1. Although the QPLAD implementation assumes that bias adjustment was performed at a coarser resolution than the target resolution for downscaling, one could apply QPLAD to unadjusted GCM simulations as well.

305 As in bias adjustment, we use a rolling 31-day window ( $\pm 15$  days) for each day of the year over the training period for each pixel. We include the last 15 days from 1994 and the first 15 days from 2015 such that each day group contains 620 values (20 years x 31 days). We then downscale historical and future model simulation data using the QPLAD adjustment factors for each variable, model, and experiment on a per pixel / day basis. Since we use 100 empirical quantiles in QDM bias adjustment and 620 quantiles in QPLAD (each corresponding to an analog day), there is not a 1:1 match between the quantiles. Consequently, for a given day, the closest quantile in QPLAD to the quantile assigned during bias adjustment is selected from the 620 possible adjustment factors for that day of year and pixel. Figure 2 demonstrates the temporal and spatial dimensions of the QPLAD method for maximum temperatures around Miami, Florida. Panel 2a shows the sixteen spatial analogs (e.g. adjustment factors) for 15 August from the fine reference data (within one  $1^\circ$  gridcell) corresponding to  $\tau_m = 0.33$  and the location of Miami, Florida. By design, the downscaled values for these sixteen gridcells will average to the bias-adjusted value at the  $1^\circ$  resolution  $x_m$  with that quantile for that day of year. Panel 2b zooms in on Miami, Florida and shows all possible spatial analogs for the same quantile but for all days of the year. For most days of the year, the adjustment factor for that day of year is moderating the bias-adjusted value, which is expected given the coastal location of Miami and the relatively low quantile. Panel 2c shows all possible analog days for 15 August, e.g. all possible 620 analogs. Finally Panel 2d shows the bias-adjusted and downscaled time series of maximum temperatures for 2080 with the 15 August values highlighted. The analog day for that quantile is  $-1.5^\circ$



320 and was applied additively to the bias-adjusted maximum temperature value for that day, thus that is the difference between the bias-adjusted and downscaled temperatures for 15 August 2080 shown in Fig. 2d.

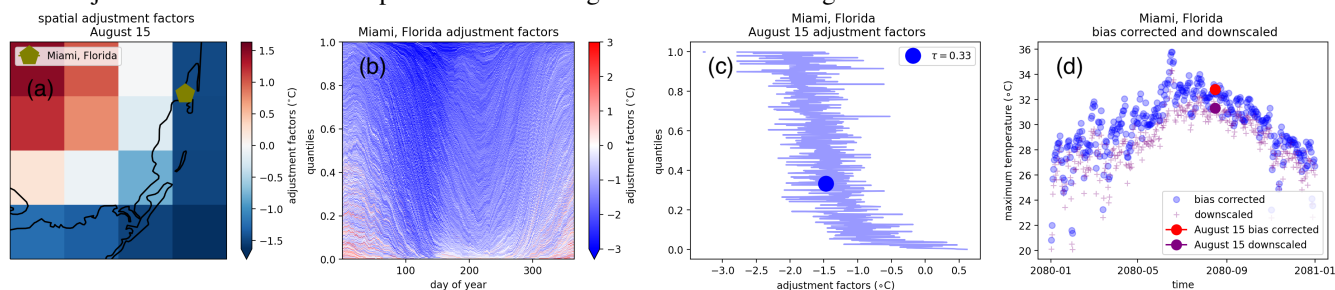


**Figure 2.** Diagram of QPLAD downscaling method. 15 August is used as an example day grouping with  $\tau = 0.33$  corresponding to the actual quantile for 15 August 2080 in the bias-adjusted output for SSP2-4.5. (a) shows spatial analogs for  $\tau = 0.33$  for 15 August, (b) shows analogs (adjustment factors) for each day of the year for Miami, Florida, (c) shows all possible adjustment factors for 15 August, and (d) shows the bias-adjusted and downscaled data for 2080 and the difference between the bias-adjusted and downscaled values for 15 August before and after the analog-based adjustment factor for  $\tau = 0.33$  has been applied. The example bias-adjusted and downscaled model data comes from the HadGEM3-GC31-LL GCM, produced by the United Kingdom Meteorological Office Hadley Centre.

330

### 4.3.1 Additional post-processing

After QPLAD downscaling, we apply an additional post-processing step that is variable-dependent. When DTR is very low in the source GCM, we found that minimum temperature may be greater than maximum temperature after downscaling. For the small number of time steps and gridcells that have this behavior, we swap maximum and minimum temperatures. We found that these conditions occurred infrequently in high-population areas, being concentrated in the polar oceans, and that this swap did not have a significant effect on seasonal or annual cycle statistics.

Precipitation requires a more complex additional bias adjustment for a limited number of grid cells and time steps globally. Adjustment factors at higher quantiles (e.g., above the 95th quantile) could become physically unrealistic when seasonal cycle behavior and precipitation magnitudes differed significantly between reanalysis reference data and the GCMs. If the GCM was biased low relative to reanalysis, this bias increased the adjustment factors further. Moreover, adjustment factors would dramatically increase if the GCM had a strong increase in precipitation signal or if values were very close to zero. However, an increasing signal did not need to be present to incur such a dramatic increase; we also found that this in the historical period outside of the training period if a given historical period either a) had a trend that was different from the training period trend or b) contained out-of-sample values that were not present in the training period. The confluence of these biases was insidious for GCMs that were downward biased relative to reference data and had seasonal precipitation cycles different than those in reference data in the same areas. This was noticeable in the intertropical convergence zone (ITCZ). To correct for these issues in a robust way, we applied a per-pixel post-downscaling adjustment factor at the target resolution that was based on the maximum

345



values of precipitation in the reference data and the fractional (SSP-dependent) increase in maximum precipitation between the historical and projected GCM simulations. Specifically, the maximum precipitation constraint for each pixel is defined as:

350

$$P_{max}(model, SSP, t) = max(P_{reference, t_1}) \times max\left(1, \frac{max(P_{model, SSP, t_2})}{max(P_{model, historical, t_1})}\right) \quad (5)$$

where  $t$  refers to a given day,  $t_1$  is defined as the training period (1995–2014),  $model$  refers to a given GCM,  $SSP$  represents one of the SSP trajectories,  $t_2$  corresponds to the maximum precipitation in a 21-year rolling window centered on the year that  $t$  is in, and  $P_{max}(model, SSP, t)$  refers to the maximum allowed precipitation at time  $t$  for a given model and SSP. Scaling by the ratio of maximum precipitation in a future 21-year rolling window to historical precipitation allows for the scaling factor to increase during the projection period if the model has an increase in the rolling 21-year maximum daily precipitation for that pixel. However, if the corresponding maximum daily precipitation decreases in the future (e.g., a scaling factor less than 1), the maximum precipitation value in the reference period for that pixel forms the constraint. After this daily constraint term is estimated for each pixel, year, experiment, and model, the final result is set equal to the minimum of the original bias-adjusted and downscaled value and this constraint.

360

#### 4.4 Transparency and reproducibility with commercial cloud computing

Our bias-adjusting and downscaling pipeline is novel because it was developed and run entirely with commercial cloud computing infrastructure. Prototypes of the pipeline were built and run on Microsoft Azure, while later production runs used Google Cloud Platform. As such, we wanted the pipeline to be reasonably replicable, open, and not bound to the proprietary hardware or software of a single cloud-computing vendor.

365

We ran steps of the pipeline in containerized software applications. These containers are a common way to hold software applications with their dependencies so that the application can run reliably on different machines. We orchestrate the containers with Argo Workflows (<https://argoproj.github.io/argo-workflows/>) on Kubernetes (<https://kubernetes.io/>), an open-source platform for managing containerized applications on a robust computer cluster that can quickly scale up or down depending on the computing resources needed. Kubernetes is ubiquitous across cloud vendors, helping us to avoid vendor lock-in. The source code for the containers and manifests orchestrating the workflow steps are both available online under an open-source license in public GitHub repositories.

370

Infrastructure is an additional challenge as it can be practically impossible to make cloud infrastructure truly replicable because commercial cloud vendors iterate their products and platforms very quickly. Despite this, we wanted to be transparent about the cloud infrastructure used for the most intense stages of this pipeline. We provisioned and configured the cloud infrastructure and the Kubernetes clusters from the project's public GitHub repository. This means that pipeline infrastructure and configuration were stored as code and automatically provisioned directly from the repository. We provisioned Google Cloud and Azure resources, including storage and a Kubernetes cluster, using Terraform (<https://www.terraform.io/>). Terraform is a common open-source tool for provisioning computer infrastructure. Once provisioned, the software on the Kubernetes

375



380 clusters was managed with ArgoCD (<https://argo-cd.readthedocs.io>), another open-source tool to deploy Kubernetes resources from the repository in near real-time.

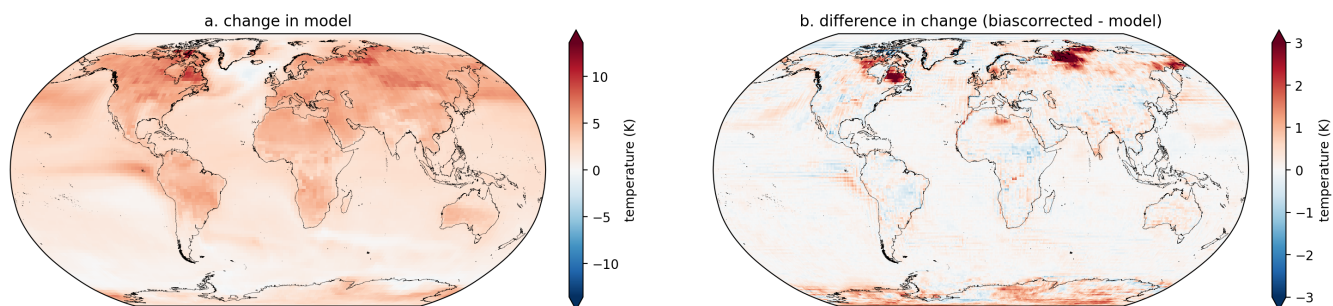
## 5 Results

In this section, we assess the robustness and performance of the QDM and QPLAD methods. First, we examine behavior in high seasonal quantiles outside of the time windows at which, by design, absolute or relative (for an additive or multiplicative  
385 variable, respectively) changes are preserved. Next, we look at the method's performance over highly populated cities and regions that are particularly important for impacts research. We explore how bias-adjustment and downscaling change the historical distribution relative to the reference distribution, and how trends are preserved for select cities across the globe. We then turn to understanding the performance of the method, specifically around trend modification, for moderate and more extreme climate indices as well as seasonal and annual aggregated metrics commonly used in impacts analysis, including  
390 seasonal mean maximum and minimum temperature and seasonal and annual total precipitation. We examine the performance of the QDM-QPLAD methods for these metrics first for a coastal city (Miami, Florida) and then at the state and country level, which we then weight by population.

### 5.1 Preserving quantile trends globally

One of the key advantages of the QDM method is its ability to preserve changes in daily model-projected extremes due to  
395 how the method imposes the model-projected change for each quantile, rather than purely the mean (e.g., standard quantile mapping). The QPLAD method provides an additional fine-scale analog-based adjustment factor approach to layering on analog day extremes present in the fine-scale reference data. Notwithstanding, it is expected that the methods will not perfectly preserve GCM-projected changes at a temporal aggregation different from that which the methods were applied. In other words, since our empirical CDFs are computed for each day of year with a 31-day window, the GCM data distributions are  
400 adjusted with the same grouping. Similarly, model-projected changes, computed as the difference or ratio between a rolling 21-year average and the historical period, will be preserved as applied. Consequently, examining temporal aggregations outside of these windows will show behavior that may dampen or inflate model-projected changes in the low and high quantiles to a minor degree. However, with a 21-year grouping of any 31-day window, corresponding to the QDM and QPLAD method-specified temporal grouping, model-projected trends would be preserved exactly. In this section, we examine trend preservation in higher  
405 quantiles at a seasonal frequency. Figure 3 shows for a selected model (NorESM2-LM) the change in the 95th percentile Northern Hemisphere summer (JJA) maximum temperature days between 2080–2100 and the historical period (1995–2014) in the source model data (a) and in panel (b) the difference in this change between the bias-adjusted model data and the source model data for the same time period and percentile.





410 **Figure 3.** Change in 95th percentile JJA maximum temperature trends globally between 2080–2100 and the training period (1995–2014) in the model (a) and the difference in this trend between the bias-adjusted data and the model (b). Results are shown for the model NorESM2-LM and the scenario SSP3-7.0.

The bias-adjusted data shown in Fig. 2b was post-processed according to the approach described in the methods section  
 415 so that it is consistent with the bias-adjusted and downscaled data. As noted above, it is expected that there will be slight modifications in the model-projected changes, Moreover, here we show the analytical 95th percentile of Northern Hemisphere (NH) summer days, rather than an empirical CDF that corresponds to the actual bias-adjustment applied. Additionally, the bias-adjusted data is at a  $1^\circ$  resolution, whereas the downscaled data is at a  $0.25^\circ$  resolution, so the bias-adjusted data is coarser and, by construction, less extreme than the downscaled data. Indeed, parts of eastern Canada and Siberia exhibit amplifications  
 420 in maximum temperature trends at the 95th percentile, as well as Antarctica. Much of these high-latitude areas that show amplification are also areas where the GCM-projected change in temperature is already high relative to other parts of the globe, consistent with the Arctic amplification that is already underway due to climate change (Previdi et al., 2021). We can infer that adjusting the GCM distribution to be consistent with the reference dataset is also contributing to this amplification of NH summer maximum temperatures. Supplemental figure 2 shows the difference in change between the bias-adjusted data  
 425 and bias-adjusted and downscaled data, and in comparing that to Fig. 3b we can infer that the amplification in model-projected changes is happening at the bias-adjustment step rather than the downscaling step, which figure A2 further confirms. However, amplification is generally very small in comparison to the actual magnitude of change projected by the model (3a) in those areas.

Precipitation has a similar but more nuanced and complex story. A longstanding challenge with bias adjustment of precipi-  
 430 tation at a global scale is dealing with the disagreement in the seasonal migration and magnitude of precipitation in the intertropical convergence zone (ITCZ) between reanalysis and GCMs. The ITCZ is a tropical “belt” where deep convection and heavy precipitation occur due to convergence of the trade winds, and the belt of heavy precipitation migrates between  $9^\circ\text{N}$  and  $2^\circ\text{N}$  as a result of annual warming of sea surface temperatures (van Hengstum et al., 2016). GCMs still exhibit bias in simulating tropical precipitation and this bias differs widely between CMIP6 models (Hagos et al., 2021; Tian and Dong, 2020). Figure  
 435 4 shows 95th percentile NH summer daily precipitation for the same model and scenario (SSP3-7.0). Panels A and B show 95th percentile seasonal Northern Hemisphere summer precipitation for the reference and the source model data respectively,



over the historical period. Panel C shows the model-projected change in 95th percentile NH summer precipitation between 2080–2100 and the historical period in the source model. Finally, panels D and E show the ratio of the bias-adjusted data to the source model data trends the ratio of the bias-adjusted and downscaled data to the bias-adjusted data, respectively. The NH summer ITCZ is pronounced and markedly different in panels A and B; for this particular GCM and percentile, differences are notable in both the shape (e.g., the ITCZ is shifted southwards in the GCM off the Brazilian coast, relative to reanalysis) and the strength of the ITCZ (e.g., the GCM overestimates the intensity of the summer monsoon over southeastern Asia and in particular over India). These biases result in slight modifications in preserving GCM-projected relative changes in the quantiles. For example, panel 4D shows that inland and just off the coastlines of India, the bias adjustment amplifies the projected change from the source GCM. Mechanically, because we choose to consider relative changes, the areas exhibiting the largest relative trends (panel C) or trend alterations (panel D) are also the driest areas (e.g. Brazil, Namibia, the Arabic peninsula in panel D). Finally, it appears, as expected, that statistical downscaling is not significantly altering the model-projected relative change signals (panel E) in comparison to the bias adjustment step, as we noted for temperature as well.

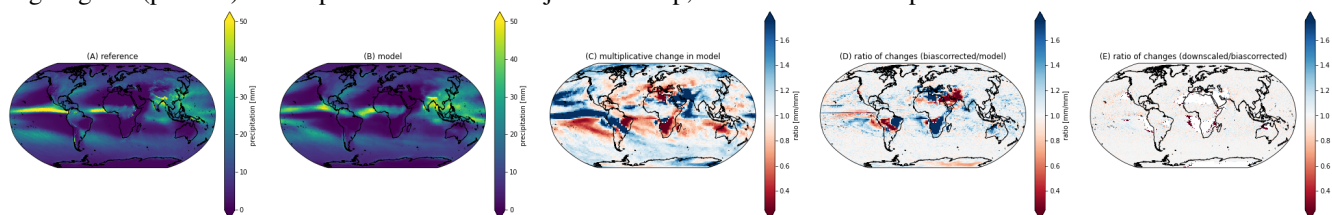


**Figure 4.** 95th percentile JJA precipitation over the historical (1995–2015) period in the reference data (A) and in the model data (B), along with the relative change, of the percentile in the 2080–2100 period to the same percentile in the historical period in the model data (C), ratio of the relative change in the bias-adjusted data to the relative change in the model data (D), ratio of the relative change in the bias-adjusted and downscaled data to the relative change in the bias-adjusted data (E). White areas in panel (E) are due to values equal to zero in the bias-adjusted and downscaled data in the historical period after the post-processing described in the methods section is applied. Results are shown for the model NorESM2-LM and the scenario SSP3-7.0.

## 5.2 Historical and future method performance for selected cities and regions

We further quantify the bias adjustment and trend preservation, here for selected aggregations and areas. Following the analysis in Bürger et al. (2012) and Cannon et al. (2015), we assess the performance of the QDM method by comparing the distributions of various CCI/CLIVAR/JCOMM Expert Team on Climate Change Detection and Indices (ETCCDI) metrics (Karl et al., 1999) metrics as well as other aggregated metrics widely used in impacts research (Table 2) over the historical period in the bias-adjusted and downscaled model data against their distribution in the reanalysis dataset, for a single city. The selected indices encompass maximum and minimum temperatures and total precipitation, ensuring that all variables included in the GDPCIR dataset are tested. We examine the performance of these metrics across all models, given the heterogeneity of temperature and



precipitation signals among models. Then, we focus on a single model, a selection of 17 metropolises globally along with their corresponding lower resolution regions and assess both bias adjustment and trend preservation.

### 5.2.1 Historical extremes indices

To check the historical distributions of the downscaled models, we examine “moderate” and “extreme” extremes detailed in  
470 Table 2 by computing the selected indices on an annual basis over the training period and over a separate validation period  
for the raw GCM, downscaled GCM and reanalysis for a single city, Miami, Florida. The chosen metrics are checks on the  
distributions of all variables included in the dataset. Some of the metrics, such as summer days, tropical nights, and annual wet  
days represent more moderate extremes less affected by threshold behavior. Others, such as consecutive dry days, days over  
35°C, and days over 32.2°C, are more affected by threshold behavior. Others, such as seasonal temperature means and total  
475 precipitation, while not classified as ETCCDI indices, are widely used as input data to sector-specific impacts modeling and  
thus are included here to guide users of the dataset.

We calculated distributions of the indices on the raw GCM output and on the bias-adjusted and downscaled GCM and each  
are compared against the reanalysis distribution of the same index using a two-sample Kolmogorov-Smirnov (K-S) test at a  
0.05 significance level. The null hypothesis is that the two samples (e.g. raw GCM and reanalysis or downscaled GCM and  
480 reanalysis) are drawn from the same distribution. A model is considered to pass the K-S test, either for the raw GCM or the  
downscaled GCM, if the null hypothesis is not rejected, in other words, if the p-value < 0.05. This is a slight modification of  
the usage of K-S tests in Cannon et al. (2015) and Bürger et al. (2012), where the authors use the D statistic rather than the  
p-value as a diagnostic. The p-value is used here for significance due to the effects of disagreement in seasonality between  
reanalysis and the GCM on the D statistic versus the p-value. We compute the K-S tests over two time periods: a calibration  
485 period (1995–2014) and a validation period (1979-1994). The validation period used is shorter because aggregated reanalysis  
data was only available from 1979 to near-real-time and had not yet been extended back to 1950 by ECMWF and made avail-  
able when hourly data was first downloaded and aggregated to daily for use in the bias adjustment and downscaling pipeline.  
For metrics that use precipitation data, the validation period is 1984–1994, because quality control showed that precipitation  
data for 1983 contained errors.

490

In Figure 5, the results of the K-S tests for the twelve selected indices for a single city, Miami, Florida, are shown for the  
downscaled and raw GCMs for the calibration and validation periods. The selected index that never passes K-S tests is frost  
days (the number of annual days below the freezing point) because there are so few years in the historical period in both  
the raw GCMs and the reanalysis that contain days below freezing. Prior to bias adjustment and downscaling, around half of  
495 the GCMs pass K-S tests in the calibration period, and afterward, all GCMs pass the K-S tests except for frost days. During  
the validation period, a considerably smaller number of K-S tests pass in the raw GCMs, while all pass after bias adjustment  
and downscaling, showing that the distributions of the selected moderate and extreme metrics have been effectively adjusted  
by the bias adjustment and downscaling algorithms. A few models are notable in the lack of passing K-S tests before bias  
adjustment and downscaling, including the BCC-CSM2-MR, GFDL-ESM4, and CCMC-ESM2 models. By contrast, INM-



500 CM4-8 is notably high before downscaling in the calibration period, indicating that its distributions of moderate and more  
extreme extrema were already closer to reanalysis for this location prior to bias adjustment. It is worth noting that because the  
location shown here is a coastal city, the additional benefit of downscaling versus solely bias adjustment is more profound, and  
thus the adjusted distributions shown here benefit both from QDM and QPLAD adjustments. Had an inland city been shown,  
the additional effect of downscaling in adjusting the distributions to the higher-resolution reanalysis distribution would have  
505 likely been less significant (unless it were in an area with complex topography).

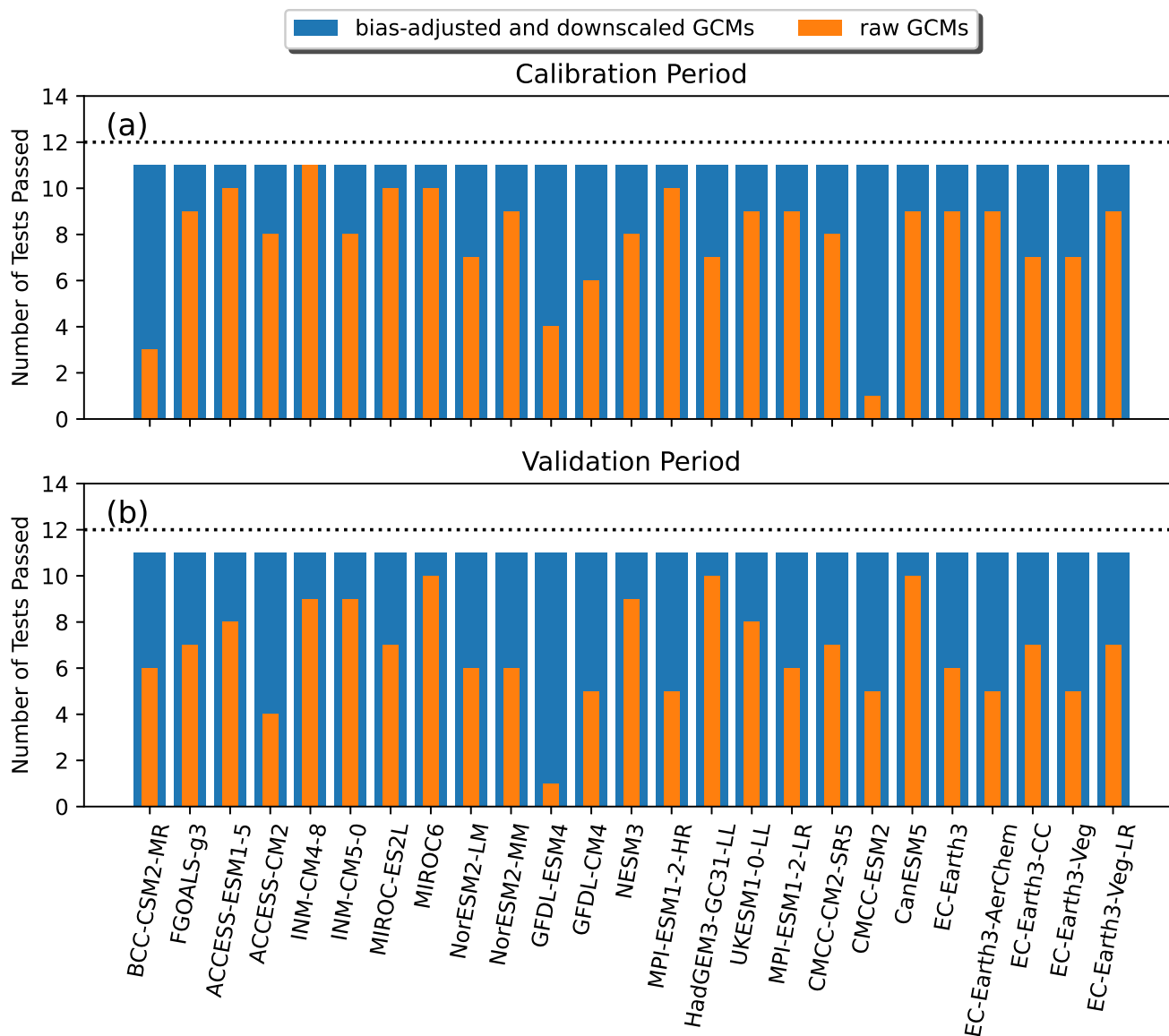


**Figure 5.** Bar plot showing the number of K-S tests passed for the twelve selected indices for the downscaled model and raw model (overlain) for each of the GCMs included in the GDPCIR dataset for a single coastal city, Miami, Florida (USA). The calibration period is shown in (a) and the validation period in (b). The dashed line shows the maximum possible number of K-S tests.



Index	Description	Surface Variable
tx_days_above	Annual count of days when daily maximum temperature > 25°C	maximum temperature
tn_days_above	Annual count of days when daily minimum temperature > 20°C	minimum temperature
wet_days	Annual count of wet days (daily total precipitation > 1.0mm)	total precipitation
wet_days_prop	Annual count of moderate precipitation days (daily total precipitation > 10.0mm)	total precipitation
seasonal minimum temperature	Mean seasonal minimum temperature for each year	minimum temperature
seasonal maximum temperature	Mean seasonal maximum temperature for each year	maximum temperature
seasonal precipitation	Total precipitation summed over seasons each year	total precipitation
annual precipitation	Annual precipitation	total precipitation
days over 32.2°C	Annual number of days over 90°F	maximum temperature
days over 35°C	Annual number of days over 95°F	maximum temperature
frost days	Annual number of days under 0°C	minimum temperature
consecutive dry days	Annual maximum number of consecutive dry days (daily total precipitation < 1.0mm)	total precipitation

**Table 2.** Selected moderate and extreme metrics for analyzing bias adjustment and downscaling algorithm performance over cities and admin1 (state/province) regions.

### 5.2.2 Bias adjustment and relative trend preservation

To further examine the performance of the bias adjustment and downscaling algorithms, we examine seasonal aggregated metrics (mean maximum and minimum temperature and total precipitation) across selected highly populated cities globally for a single model, BCC-CSM2-MR, by computing the median absolute error in bias adjustment compared to the mean seasonal error in trend preservation between the raw and downscaled GCMs. Following the method used by Lange (2019), we define absolute error in bias adjustment as:

$$e = |y_{hist}^{sim} - x_{hist}^{obs}| \tag{6}$$



where  $y_{hist}^{sim}$  represents bias adjusted historical simulations and  $x_{hist}^{obs}$  represents historical reference data. We then define absolute error in trend preservation as:

$$515 \quad e = |(y_{fut}^{sim} - y_{hist}^{sim}) - (x_{fut}^{sim} - x_{hist}^{sim})| \quad (7)$$

where  $y_{fut}^{sim}$  represents bias adjusted projections,  $y_{hist}^{sim}$  represents bias adjusted historical simulations,  $x_{fut}^{sim}$  represents future projections (unadjusted) and  $x_{hist}^{sim}$  represents historical simulations (unadjusted).

However, we depart from the Lange (2019) method by computing the absolute error over seasonal means or sums (for temperature and precipitation, respectively) and for cities globally rather than at multiple spatial resolutions. Because we are  
520 computing the error on an annual basis rather than over a 21-year rolling window, the difference in trend between the raw GCM and downscaled GCM is non-zero (our QDM implementation perfectly preserves relative seasonal trends between a given future 21-year rolling window and the historical training period). Figure 6 shows these results over selected cities globally. Overall, bias-adjustment and trend-preservation errors are lower for minimum temperature than for maximum temperature but are generally low for both surface variables. Bias adjustment error for precipitation is low for the majority of cities with the  
525 notable exception of São Paulo, which has a median error of over 14. This comparatively larger error in bias adjustment can be explained by both a) a difference in seasonal precipitation magnitudes for that location in reanalysis vis-a-vis the GCM, and b) significantly larger interannual variability for São Paulo versus other cities shown. A shortcoming of only showing bias-adjusted and downscaled error in Figure 6 versus also showing the same analysis for bias-adjusted data for the same model and cities means that we cannot attribute the bias adjustment error in São Paulo to (a) or (b), but it is likely that both play a  
530 large role, given the issues with precipitation in the tropics discussed earlier. In Lange (2019), the author conducted similar error analysis for surface variables over different CMIP5 GCMs (MIROC5, IPSL-CM5A-LR, and GFDL-ESM2M) at a coarser resolution ( $2^\circ$ ) and found similar magnitudes of error in trend preservation, with slightly smaller errors in bias adjustment. The larger values in bias adjustment shown here are likely due to the fact that the errors are being calculated at a higher resolution for cities (with raw GCM, reanalysis, and downscaled data drawn from the nearest  $0.25^\circ$  gridcell) and thus there are larger  
535 errors between the coarse-resolution GCM and the higher-resolution reanalysis, and the preservation of climate change signal in quantiles is implemented on a 21-year rolling window in our study.

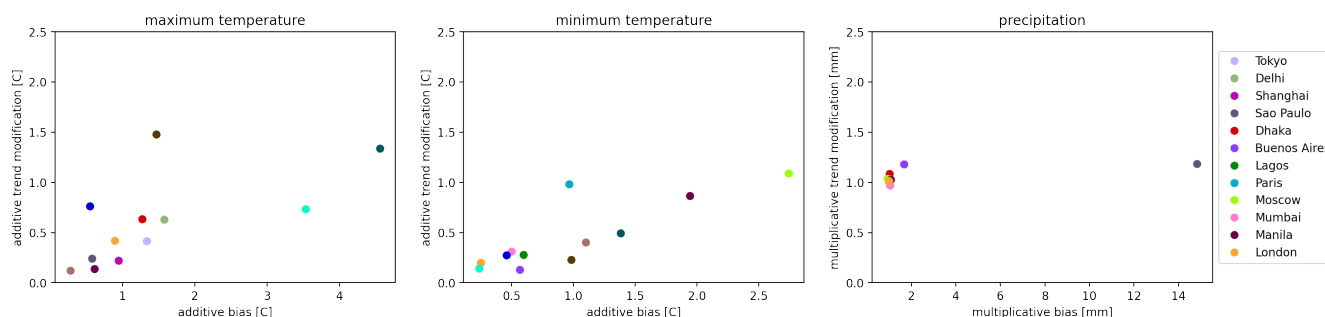


**Figure 6.** Efficacy of bias adjustment and relative trend preservation for seasonal maximum and minimum temperature and seasonal total precipitation computed annually for a single GCM (BCC-CSM1-2) for selected highly populated cities globally. The historical period used is 1995-2014, while the projection period is SSP3-7.0 2080-2100. More precisely, for temperature variables, the values on the x-axis are the median over the seasonal absolute (additive) bias adjustment errors, and the values on the y-axis are the median over the seasonal absolute (additive) error in (additive) trend preservation. For precipitation, errors are multiplicative and instead of taking the mean over seasons, we take the sum over seasons.

### 5.2.3 Relative trend preservation in selected regions

One of the key considerations in developing a method and dataset for use in the study of the human impacts of climate change is the performance of the given method when the data is reconfigured, transformed, or re-weighted by the users of the data. Impacts research frequently uses weighted, aggregated extreme value measures, such as crop-output-weighted frost-day counts for a given agricultural zone, or population-weighted counts of hot nights for a given census region. To understand the performance of our data under such circumstances, we use the same set of diagnostic cities examined above to understand preservation of moderate and extreme trends for several of the moderate and extreme ETCCDI indicators at varying levels of aggregation. Following the regional aggregation method described in Rode et al. (2021), these comparisons use a 30-arcsecond population raster dataset (CIESIN, 2018) to determine the weight of each grid cell in the climate dataset within each region's total, based on whether the population grid cell is contained within each region's shapefile. Data is aggregated to either admin0 or admin1 regions after computing the ETCCDI metrics on gridded data. An admin1 region is a generic term that refers to the largest subnational administrative unit of a country; for example, a state in the US or a prefecture in Japan. An admin0 region refers to national boundaries, e.g. the US or Japan. Shapefiles that define these region boundaries are taken from the Natural Earth dataset (Earth, 2022), and are further subset to include the admin0 or admin1 region which includes each of the diagnostic cities listed above.

For the analysis in this section, we use the same temporal aggregation as in the method implementation such that any modification of trend is not due to the effects described earlier but instead due to aggregation or weighting effects. Because the method exactly preserves quantile trends within a 31-day window during bias adjustment, and preserves trends in minimum tempera-





ture, maximum temperature, and log(precipitation) for a given quantile on an average basis across  $0.25^\circ$  gridcells within each coarse  $1^\circ$  cell, discrepancies between trends in seasonal and annual mean minimum temperature and maximum temperature are due solely to differences between area and population weights, and due to the effects of Gaussian interpolation from the native GCM grid to the regular  $1^\circ$  grid used for bias adjustment. This behavior can be seen in the very high degree of agreement  
 560 between source GCM and bias adjusted and downscaled trends at both the admin0 and admin1 level for maximum temperature in Figure 7. Here, we calculate trend using the difference between the 1995-2014 period average and the 2079-2099 period average; the year 2100 is not included because it is not available in all GCMs. Panels a-e in Figure 7 show the change in period average annual and seasonal maximum temperature for admin0 regions (e.g. countries) and for admin1 regions (e.g. states/provinces) in panels f-j. The admin0 and admin1 regions shown correspond to the regions where each of the cities is  
 565 located, and results are shown for all GCMs and all scenarios (SSP1-2.6, SSP2-4.5, SSP3-7.0 and SSP5-8.5). Both admin0 and admin1 regions have an  $r^2$  value of at least 0.9 for both annual temperature and all seasons, showing extremely minimal trend modification.

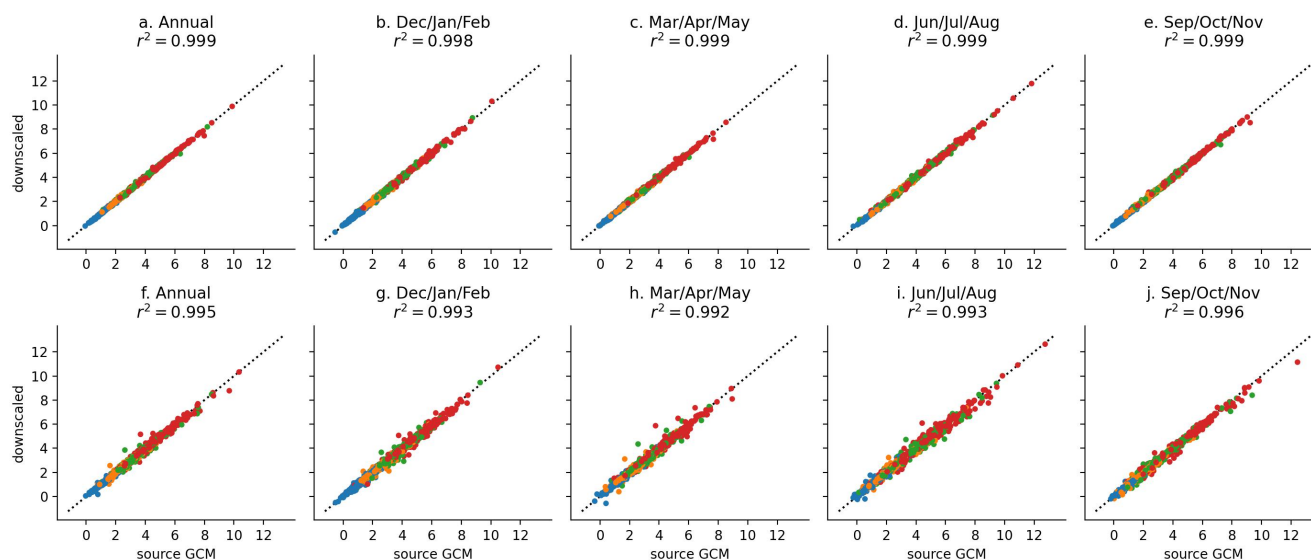


**Figure 7.** Change in period average annual and seasonal maximum daily  $T_{max}$  from 1995-2014 to 2079-2099, for countries (top row; panels a-e) and states/provinces (bottom row; panels f-j) containing the 17 diagnostic cities. All GCMs and scenarios are shown; with SSP1-2.6 (blue), SSP2-4.5 (orange); SSP3-7.0 (green), and SSP5-8.5 (red).

However, because precipitation adjustments are multiplicative, 21-year seasonal and annual totals are not preserved exactly when aggregated. Fidelity to the source model trend in the downscaled data is closer when comparing trends in log(21-year  
 570 annual average precipitation) or log(21-year seasonal average precipitation), which can be seen in comparing the first and second rows in Figure 8. Figure 8 shows annual and seasonal precipitation for the countries containing the 17 selected global cities for all GCMs and scenarios, with the change in period average precipitation shown in panels a-e and log(period average



annual and seasonal precipitation) in panels f-j. As expected the higher emissions scenarios SSP3-7.0 and SSP5-8.5 appear far more often as outliers, which is expected given their relatively larger change signals in precipitation.

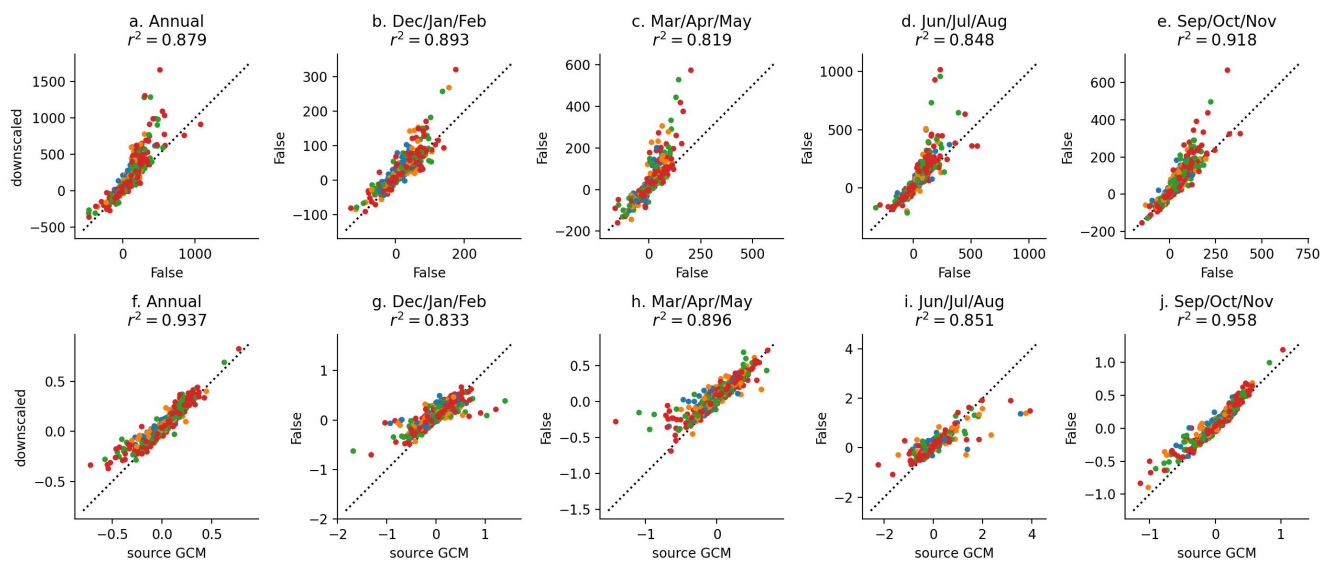


**Figure 8.** Change in period average annual and seasonal precipitation from 1994-2014 to 2079-2099, (top row; panels a-e) and the change in log(period average annual and seasonal precipitation) (bottom row; panels f-j) for the countries containing the 17 diagnostic cities. All GCMs and scenarios are shown; with SSP1-2.6 (blue), SSP2-4.5 (orange); SSP3-7.0 (green), and SSP5-8.5 (red).

575 To understand trend preservation among extreme metrics, we computed the count of days above or below various thresholds, shown in Figure 9. The method does not explicitly preserve the GCM signal in such metrics, as anomalies in temperatures, even at extreme quantiles, will cross a threshold with different frequencies after a linear or multiplicative adjustment. This behavior is consistent with the fact that, while trends in extreme values measured as quantiles will be preserved within any 31-day window from the GCM to the final result, trends in any absolute measure, such as counts of days above or below a

580 threshold, will be affected by the bias adjustment and may be significantly different in the result depending on the metric.

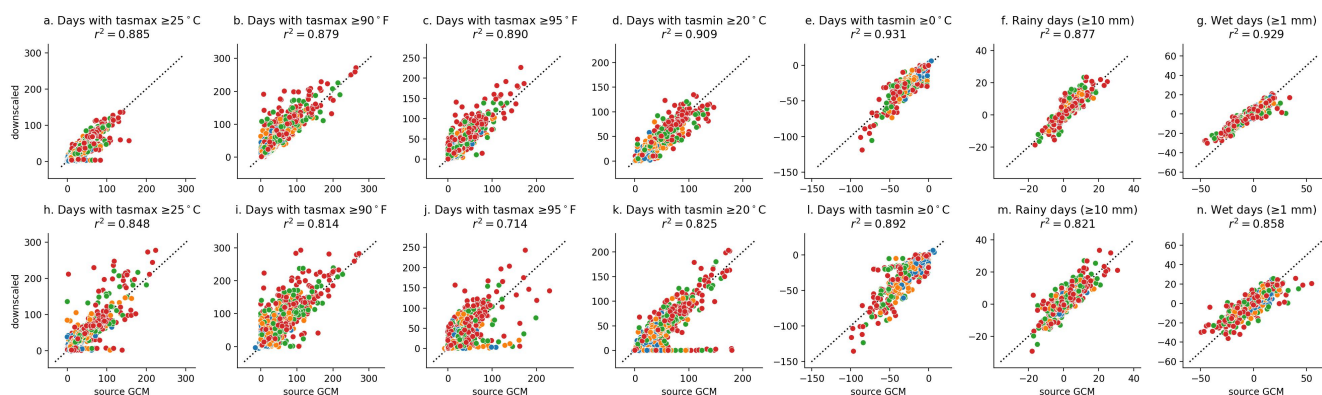


**Figure 9.** Change in period average threshold counts from 1994-2014 to 2079-2099, for countries (top row; panels a-g) and state/provinces (bottom row; panels h-n) containing the 17 diagnostic cities. All GCMs and scenarios are shown; with SSP1-2.6 (blue), SSP2-4.5 (orange); SSP3-7.0 (green), and SSP5-8.5 (red).

## 6 Conclusions

We hope that the GDPCIR dataset will be a useful contribution for climate impacts research in its scope, resolution and in the methods applied that were specifically tailored to understanding the tail risks associated with future emissions pathways. The QDM-QPLAD bias adjustment and downscaling algorithms preserve quantile trends and therefore allow users to better understand and model the effects of different emissions pathways on sector-specific and aggregate climate impacts. The 0.25° resolution of the GDPCIR dataset allows for its use in econometric models that require high-resolution surface climate data for estimating response functions. Errors in bias adjustment and trend preservation are low, with some exceptions for precipitation due to issues already discussed. Figure A1 goes into further detail on this. We expect that the dataset will have broad use in a variety of climate impacts modeling, from estimating econometric dose-response functions to hydrology and ecology to modeling ecosystem services and natural capital.

*Code availability.* The R/CIL GDPCIR dataset codebase containing notebooks, pipeline architecture, and infrastructure is publicly available at <https://github.com/ClimateImpactLab/downscaleCMIP6> and archived at <https://doi.org/10.5281/zenodo.6403794>. The software container and all code used for individual downscaling pipeline tasks is publicly available at <https://github.com/ClimateImpactLab/dodola> and archived at <https://doi.org/10.5281/zenodo.6383442>, and our production pipeline was run with release v0.19.0.



*Data availability.* The GDPCIR dataset is publicly hosted on the Microsoft Planetary Computer (<https://planetarycomputer.microsoft.com/dataset/group/cil-gdpcir/>).

## Appendix A: Supplementary figures

### A1 Global temperature and precipitation changes

600 In this section we explore trends in global temperature and precipitation across models. We report these trends for both the  
source data and the bias-adjusted and downscaled data in order to shed light on how these global trends are affected by QDM  
and QPLAD. To obtain global values, the data is averaged using land-weighting. Results are shown in Fig A1. We find that  
when comparing the source data with the bias-adjusted and downscaled data, global trends in temperature are preserved: all  
the differences across models and scenarios are within  $\pm 0.1^\circ\text{C}$ . In contrast, changes in global precipitation have some amount  
605 of inflation across all models and scenarios. Going further, in the SSP2-4.5 and SSP3-7.0(respectively) source data, change  
in average annual mean maximum temperature across models ranges from  $1.71^\circ\text{C}$  ( $2.56^\circ\text{C}$ ) to  $4.55^\circ\text{C}$  ( $6.53^\circ\text{C}$ ) and in the  
bias-adjusted downscaled data this range is almost identical, from  $1.71^\circ\text{C}$  ( $2.84^\circ\text{C}$ ) to  $4.55^\circ\text{C}$  ( $6.54^\circ\text{C}$ ). In contrast, change in  
average annual total precipitation ranges from  $-0.11\%$  ( $-2.47\%$ ) to  $8.99\%$  ( $9.61\%$ ) in the source data and is shifted upwards in  
the bias-adjusted and downscaled data, from  $2.57\%$  ( $-0.79\%$ ) to  $12.6\%$  ( $15.22\%$ ). For precipitation, the largest change is in the  
610 scenario SSP3-7.0, CanESM5 model, with a source trend of around  $7.5\%$  and a trend in our results of  $15\%$ . This model also has  
one of the highest precipitation trends in the source data, but there is no systematic relationship between the magnitude of the  
source trend and the magnitude of trend modification. For example, NorESM2-MM SSP2-4.5 has a trend close to zero in the  
source data and in the results the trend is around  $4\%$ , whereas BCC-CSM2-MR has a trend of around  $2.5\%$  in both scenarios  
and the alteration is very low at less than  $0.2$  percentage points in both scenarios.

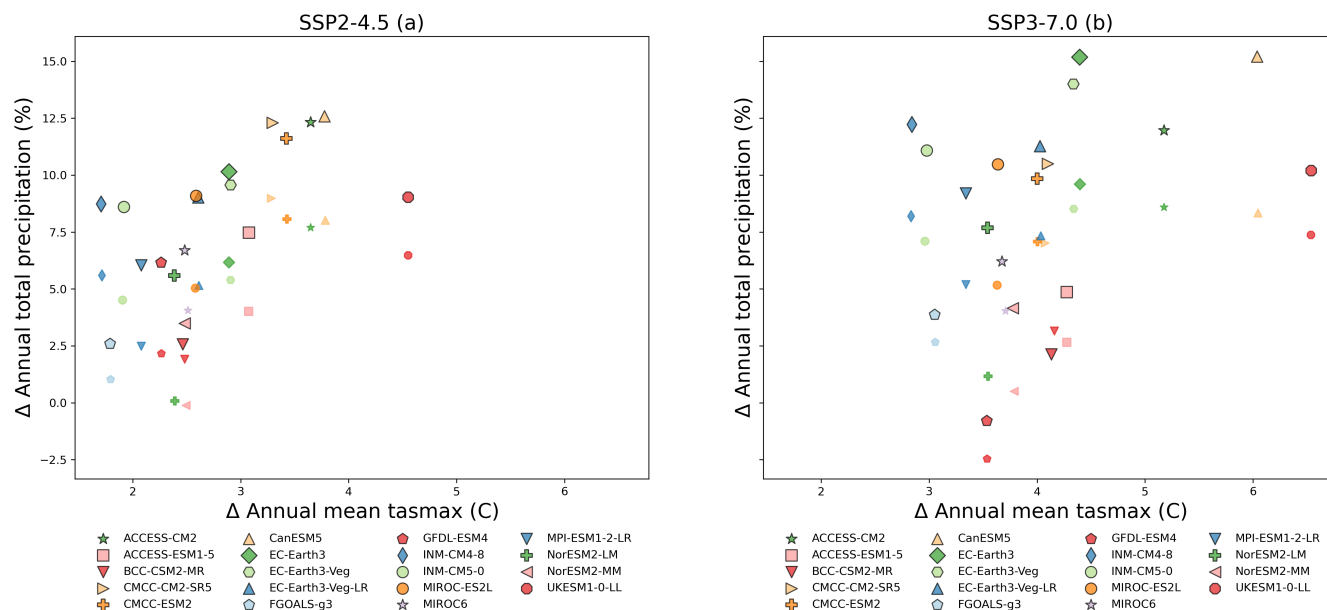
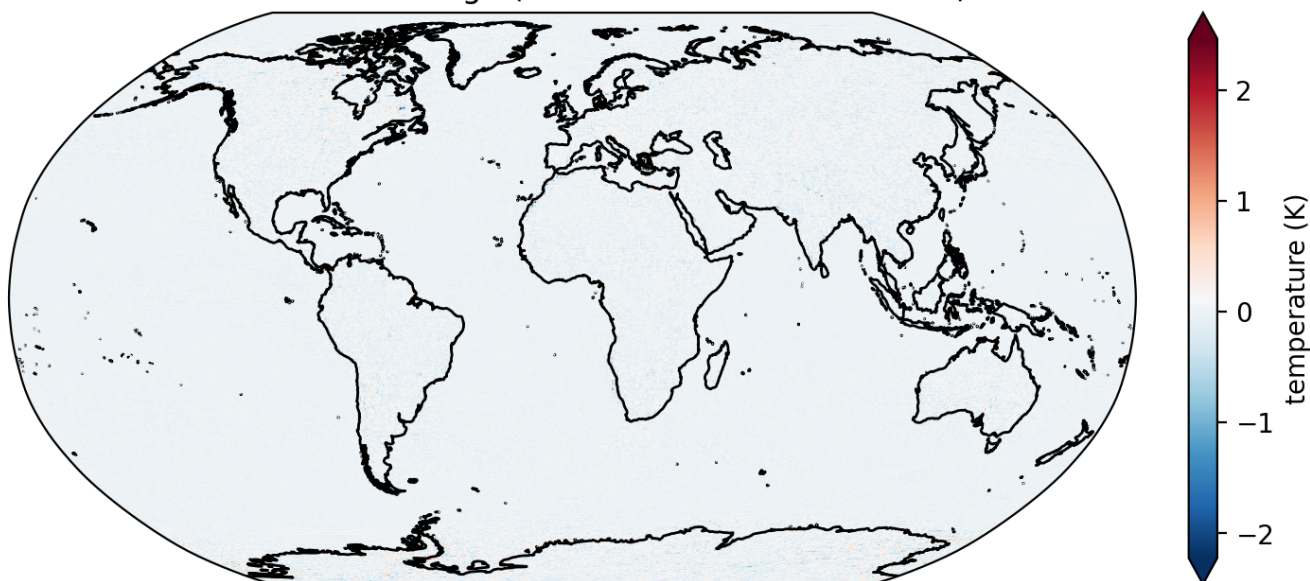


**Figure A1.** Changes in temperature and precipitation signals in CMIP6 source models and CMIP6 bias-adjusted and downscaled models. For each model, scenario and pixel, the annual average (x-axis) and the annual total (y-axis) is computed for each year of both the historical (1995-2015) and future (2080-2100) period. Then, the data is averaged over space with a land-weighting scheme (e.g. ocean pixels are assigned zero weights). Finally, the data is averaged over years for both the historical and future period separately and the difference between the future and historical global values (x-axis) or the percent change between the future and the historical global values (y-axis) is plotted. Data point symbols with transparent borders represent the source model data while those with black color borders represent the bias-adjusted and downscaled data. The list of models is restricted to those that have bias-adjusted and downscaled data for both SSP2-4.5 and SSP3-7.0.



difference in change (downscaled - biascorrected)



615

**Figure A2.** Difference in the change in 95th percentile JJA maximum temperature trends globally between 2080-2100 and the training period (1995-2014) between the bias-adjusted and downscaled data and the bias-adjusted data. Results are shown for the model NorESM2-LM and the scenario SSP3-7.0.

620 *Author contributions.*

DRG led the design, methods development and collaborations for the CMIP6 downscaling project and also contributed extensively to code development and pipeline architecture. SBM was the lead data scientist and engineer, developed our downscaling pipeline and also contributed to methods development. KEM and MTD contributed to method and code development throughout the project. ET worked on code development and helped with production runs and later worked on analysis and QC of results. MAF led analysis and preparation of ERA5 reanalysis data for the production pipeline. REK provided technical advice and oversight on the project throughout.

625 DRG wrote the first complete draft of the article with contributions from SBM (reproducibility section) and MTD (results aggregated to state and country levels). DRG, ET, MTD and KEM made all figures. REK provided an extremely thorough review. DRG revised the article, iteratively with comments from KEM, ET and SBM.

630 *Competing interests.*



The authors declare that no competing interests are present.

*Acknowledgements.* The authors acknowledge the World Climate Research Programme's Working Group on Coupled Modelling, which is responsible for CMIP, and would like to thank the climate modeling groups for producing and making available their model output. They would further like to thank Lamont-Doherty Earth Observatory, the Pangeo Consortium, Google Cloud, and the Google Public Datasets program for making the CMIP6 Google Cloud collection possible. In particular, the authors would like to express gratitude to Ryan Abernathey, Naomi Henderson, and Charles Blackmon-Luca for ongoing collaboration on making the CMIP6 Zarr stores analysis-ready. The authors are grateful to the xclim developers, in particular, Pascal Bourgault and Travis Logan, for implementing the QDM bias-adjustment method in the xclim Python package, supporting the authors' QPLAD implementation into the package, and ongoing support integrating the dask parallel computing library into downscaling workflows. For method advice and useful conversations, the authors would like to thank Keith Dixon and Dennis Adams-Smith. Thanks to Dan Morris, Tom Augspurger, and the team at Microsoft AI for Earth and Azure for help coordinating computing infrastructure, public data release, and all the subtle steps in between.

*Financial support.*

This research has been supported by the Rockefeller Foundation and the Microsoft AI for Earth Initiative.



## References

- 645 Abernathey, R. P., Augspurger, T., Banihirwe, A., Blackmon-Luca, C. C., Crone, T. J., Gentemann, C. L., Hamman, J. J., Henderson, N., Lepore, C., McCaie, T. A., Robinson, N. H., and Signell, R. P.: Cloud-Native Repositories for Big Scientific Data, *Computing in Science & Engineering*, 23, 26–35, <https://doi.org/10.1109/MCSE.2021.3059437>, 2021.
- Agbazo, M. N. and Grenier, P.: Characterizing and avoiding physical inconsistency generated by the application of univariate quantile mapping on daily minimum and maximum temperatures over Hudson Bay, *International Journal of Climatology*, 40, 3868–3884, <https://doi.org/10.1002/joc.6432>, eprint: <https://onlinelibrary.wiley.com/doi/pdf/10.1002/joc.6432>, 2020.
- 650 Bürger, G., Murdock, T. Q., Werner, A. T., Sobie, S. R., and Cannon, A. J.: Downscaling Extremes—An Intercomparison of Multiple Statistical Methods for Present Climate, *Journal of Climate*, 25, 4366–4388, <https://doi.org/10.1175/JCLI-D-11-00408.1>, publisher: American Meteorological Society Section: *Journal of Climate*, 2012.
- Cannon, A. J.: Multivariate quantile mapping bias correction: an N-dimensional probability density function transform for climate model simulations of multiple variables, *Climate Dynamics*, 50, 31–49, <https://doi.org/10.1007/s00382-017-3580-6>, 2018.
- 655 Cannon, A. J., Sobie, S. R., and Murdock, T. Q.: Bias Correction of GCM Precipitation by Quantile Mapping: How Well Do Methods Preserve Changes in Quantiles and Extremes?, *Journal of Climate*, 28, 6938–6959, <https://doi.org/10.1175/JCLI-D-14-00754.1>, publisher: American Meteorological Society Section: *Journal of Climate*, 2015.
- Cannon, A. J., Piani, C., and Sippel, S.: Chapter 5 - Bias correction of climate model output for impact models, in: *Climate Extremes and Their Implications for Impact and Risk Assessment*, edited by Sillmann, J., Sippel, S., and Russo, S., pp. 77–104, Elsevier, <https://doi.org/10.1016/B978-0-12-814895-2.00005-7>, 2020.
- 660 Carleton, T., Jina, A., Delgado, M., Greenstone, M., Houser, T., Hsiang, S., Hultgren, A., Kopp, R. E., McCusker, K. E., Nath, I., Rising, J., Rode, A., Seo, H. K., Viaene, A., Yuan, J., and Zhang, A. T.: Valuing the Global Mortality Consequences of Climate Change Accounting for Adaptation Costs and Benefits, *The Quarterly Journal of Economics*, 137, 2037–2105, <https://doi.org/10.1093/qje/qjac020>, 2022.
- 665 CIESIN: Gridded Population of the World, Version 4 (GPWv4): Population Count Adjusted to Match 2015 Revision of UN WPP Country Totals, Revision 11, <https://sedac.ciesin.columbia.edu/data/set/gpw-v4-population-density-adjusted-to-2015-unwpp-country-totals-rev11>, center for International Earth Science Information Network - CIESIN - Columbia University, Palisades, NY: NASA Socioeconomic Data and Applications Center (SEDAC), 2018.
- Dai, A.: Precipitation Characteristics in Eighteen Coupled Climate Models, *Journal of Climate*, 19, 4605–4630, <https://doi.org/10.1175/JCLI3884.1>, publisher: American Meteorological Society Section: *Journal of Climate*, 2006.
- 670 Earth, N.: 1:10m Cultural Vectors, Version 5.0.1, <https://naturalearthdata.com>, 2022.
- Eyring, V., Bony, S., Meehl, G. A., Senior, C. A., Stevens, B., Stouffer, R. J., and Taylor, K. E.: Overview of the Coupled Model Intercomparison Project Phase 6 (CMIP6) experimental design and organization, *Geoscientific Model Development*, 9, 1937–1958, <https://doi.org/10.5194/gmd-9-1937-2016>, publisher: Copernicus GmbH, 2016.
- 675 François, B., Vrac, M., Cannon, A. J., Robin, Y., and Allard, D.: Multivariate bias corrections of climate simulations: which benefits for which losses?, *Earth System Dynamics*, 11, 537–562, <https://doi.org/10.5194/esd-11-537-2020>, publisher: Copernicus GmbH, 2020.
- Hacker, J.: The Essential Components of the Downscaling Toolbox, <https://jupiterintel.com/wp-content/uploads/2021/04/Jupiter-Downscaling-Science-Insights.pdf>, jupiter Intelligence Science Insights, 2021.
- Hagos, S. M., Leung, L.-Y., Garuba, O. A., Demott, C., Harrop, B. E., Lu, J., and Ahn, M.-S.: The Relationship between Precipitation and Precipitable Water in CMIP6 Simulations and Implications for Tropical Climatology and Change, *Journal of Climate*, 34,
- 680





- <https://doi.org/10.1175/jcli-d-20-0211.1>, institution: Pacific Northwest National Lab. (PNNL), Richland, WA (United States) Number: PNNL-SA-152254 Publisher: American Meteorological Society, 2021.
- Hassler, B. and Lauer, A.: Comparison of Reanalysis and Observational Precipitation Datasets Including ERA5 and WFDE5, *Atmosphere*, 12, 1462, <https://doi.org/10.3390/atmos12111462>, number: 11 Publisher: Multidisciplinary Digital Publishing Institute, 2021.
- 685 Hempel, S., Frieler, K., Warszawski, L., Schewe, J., and Piontek, F.: A trend-preserving bias correction – the ISI-MIP approach, *Earth System Dynamics*, 4, 219–236, <https://doi.org/10.5194/esd-4-219-2013>, publisher: Copernicus GmbH, 2013.
- Hersbach, H., Bell, B., Berrisford, P., Biavati, G., Horányi, A., Muñoz Sabater, J., Nicolas, J., Peubey, C., Radu, R., Rozum, I., Schepers, D., Simmons, A., Soci, C., Dee, D., and Thépaut, J.-N.: ERA5 hourly data on single levels from 1979 to present, <https://doi.org/10.24381/cds.adbb2d47>, copernicus Climate Change Service (C3S) Climate Data Store (CDS), 2018.
- 690 Holthuijzen, M., Beckage, B., Clemins, P. J., Higdon, D., and Winter, J. M.: Robust bias-correction of precipitation extremes using a novel hybrid empirical quantile-mapping method, *Theoretical and Applied Climatology*, 149, 863–882, <https://doi.org/10.1007/s00704-022-04035-2>, 2022.
- Karl, T. R., Nicholls, N., and Ghazi, A.: Clivar/GCOS/WMO Workshop on Indices and Indicators for Climate Extremes Workshop Summary, *Climatic Change*, 42, 3–7, <https://doi.org/10.1023/A:1005491526870>, 1999.
- 695 Lange, S.: Trend-preserving bias adjustment and statistical downscaling with ISIMIP3BASD (v1.0), *Geoscientific Model Development*, 12, 3055–3070, <https://doi.org/10.5194/gmd-12-3055-2019>, publisher: Copernicus GmbH, 2019.
- Lanzante, J. R., Adams-Smith, D., Dixon, K. W., Nath, M., and Whitlock, C. E.: Evaluation of some distributional downscaling methods as applied to daily maximum temperature with emphasis on extremes, *International Journal of Climatology*, 40, 1571–1585, <https://doi.org/10.1002/joc.6288>, eprint: <https://onlinelibrary.wiley.com/doi/pdf/10.1002/joc.6288>, 2020.
- 700 Lehner, F., Nadeem, I., and Formayer, H.: Evaluating quantile-based bias adjustment methods for climate change scenarios, *Hydrol. Earth Syst. Sci. Discuss.*, 2021, 1–26, <https://doi.org/10.5194/hess-2021-498>, publisher: Copernicus Publications, 2021.
- Logan, T., Bourgault, P., Smith, T. J., Huard, D., Biner, S., Labonté, M.-P., Rondeau-Genesse, G., Fyke, J., Aoun, A., Roy, P., Ehbrecht, C., Caron, D., Stephens, A., Whelan, C., Low, J.-F., and Lavoie, J.: Ouranosinc/xclim: v0.31.0, <https://doi.org/10.5281/zenodo.5649661>, 2021.
- 705 Maraun, D.: Bias Correcting Climate Change Simulations - a Critical Review, *Current Climate Change Reports*, 2, 211–220, <https://doi.org/10.1007/s40641-016-0050-x>, 2016.
- Maraun, D. and Widmann, M.: *Statistical Downscaling and Bias Correction for Climate Research*, Cambridge University Press, Cambridge, <https://doi.org/10.1017/9781107588783>, 2018.
- Masson-Delmotte, V., Zhai, P., Pirani, A., Connors, S. L., Péan, C., Berger, S., Caud, N., Chen, Y., Goldfarb, L., Gomis, M. I., Huang, M., Leitzell, K., Lonnoy, E., Matthews, J. B. R., Maycock, T. K., Waterfield, T., Yelekçi, Ö., Yu, R., and Zhou, B., eds.: *Climate Change 2021: The Physical Science Basis. Contribution of Working Group I to the Sixth Assessment Report of the Intergovernmental Panel on Climate Change*, Cambridge University Press, 2021.
- Maurer, E. P. and Pierce, D. W.: Bias correction can modify climate model simulated precipitation changes without adverse effect on the ensemble mean, *Hydrology and Earth System Sciences*, 18, 915–925, <https://doi.org/10.5194/hess-18-915-2014>, 2014.
- 715 Müller, C., Franke, J., Jägermeyr, J., Ruane, A. C., Elliott, J., Moyer, E., Heinke, J., Falloon, P. D., Folberth, C., Francois, L., Hank, T., Izaurrealde, R. C., Jacquemin, I., Liu, W., Olin, S., Pugh, T. A. M., Williams, K., and Zabel, F.: Exploring uncertainties in global crop yield projections in a large ensemble of crop models and CMIP5 and CMIP6 climate scenarios, *Environmental Research Letters*, 16, 034040, <https://doi.org/10.1088/1748-9326/abd8fc>, 2021.



- O'Neill, B. C., Tebaldi, C., van Vuuren, D. P., Eyring, V., Friedlingstein, P., Hurtt, G., Knutti, R., Kriegler, E., Lamarque, J.-F., Lowe,  
720 J., Meehl, G. A., Moss, R., Riahi, K., and Sanderson, B. M.: The Scenario Model Intercomparison Project (ScenarioMIP) for CMIP6,  
Geoscientific Model Development, 9, 3461–3482, <https://doi.org/10.5194/gmd-9-3461-2016>, publisher: Copernicus GmbH, 2016.
- Parsons, L. A., Masuda, Y. J., Kroeger, T., Shindell, D., Wolff, N. H., and Spector, J. T.: Global labor loss due to humid heat exposure  
underestimated for outdoor workers, *Environmental Research Letters*, 17, 014 050, <https://doi.org/10.1088/1748-9326/ac3dae>, publisher:  
IOP Publishing, 2022.
- 725 Pierce, D. W., Cayan, D. R., and Thrasher, B. L.: Statistical Downscaling Using Localized Constructed Analogs (LOCA), *Journal of Hydrom-  
eteorology*, 15, 2558–2585, <https://doi.org/10.1175/JHM-D-14-0082.1>, publisher: American Meteorological Society Section: Journal of  
Hydrometeorology, 2014.
- Previdi, M., Smith, K. L., and Polvani, L. M.: Arctic amplification of climate change: a review of underlying mechanisms, *Environmental  
Research Letters*, 16, 093 003, <https://doi.org/10.1088/1748-9326/ac1c29>, publisher: IOP Publishing, 2021.
- 730 Qian, W. and Chang, H. H.: Projecting Health Impacts of Future Temperature: A Comparison of Quantile-Mapping Bias-Correction Methods,  
*International Journal of Environmental Research and Public Health*, 18, 1992, <https://doi.org/10.3390/ijerph18041992>, 2021.
- Riahi, K., van Vuuren, D. P., Kriegler, E., Edmonds, J., O'Neill, B. C., Fujimori, S., Bauer, N., Calvin, K., Dellink, R., Fricko, O., Lutz,  
W., Popp, A., Cuaresma, J. C., Kc, S., Leimbach, M., Jiang, L., Kram, T., Rao, S., Emmerling, J., Ebi, K., Hasegawa, T., Havlik, P.,  
Humpenöder, F., Da Silva, L. A., Smith, S., Stehfest, E., Bosetti, V., Eom, J., Gernaat, D., Masui, T., Rogelj, J., Strefler, J., Drouet,  
735 L., Krey, V., Luderer, G., Harmsen, M., Takahashi, K., Baumstark, L., Doelman, J. C., Kainuma, M., Klimont, Z., Marangoni, G., Lotze-  
Campen, H., Obersteiner, M., Taboada, A., and Tavoni, M.: The Shared Socioeconomic Pathways and their energy, land use, and greenhouse  
gas emissions implications: An overview, *Global Environmental Change*, 42, 153–168, <https://doi.org/10.1016/j.gloenvcha.2016.05.009>,  
2017.
- Rode, A., Carleton, T., Delgado, M., Greenstone, M., Houser, T., Hsiang, S., Hultgren, A., Jina, A., Kopp, R. E., McCusker, K. E.,  
740 Nath, I., Rising, J., and Yuan, J.: Estimating a social cost of carbon for global energy consumption, *Nature*, 598, 308–314,  
<https://doi.org/10.1038/s41586-021-03883-8>, number: 7880 Publisher: Nature Publishing Group, 2021.
- Sanabria, L. A., Qin, X., Li, J., and Cechet, R. P.: Bias correction of extreme values of high-resolution climate simulations for risk analysis,  
*Theoretical and Applied Climatology*, 150, 1015–1026, <https://doi.org/10.1007/s00704-022-04210-5>, 2022.
- Sheffield, J., Goteti, G., and Wood, E. F.: Development of a 50-Year High-Resolution Global Dataset of Meteorological Forcings for Land  
745 Surface Modeling, *Journal of Climate*, 19, 3088–3111, <https://doi.org/10.1175/JCLI3790.1>, publisher: American Meteorological Society  
Section: Journal of Climate, 2006.
- Sillmann, J., Kharin, V. V., Zhang, X., Zwiers, F. W., and Bronaugh, D.: Climate extremes indices in the CMIP5 multimodel  
ensemble: Part 1. Model evaluation in the present climate, *Journal of Geophysical Research: Atmospheres*, 118, 1716–1733,  
<https://doi.org/10.1002/jgrd.50203>, eprint: <https://onlinelibrary.wiley.com/doi/pdf/10.1002/jgrd.50203>, 2013.
- 750 Supharatid, S., Aribarg, T., and Nafung, J.: Bias-corrected CMIP6 climate model projection over Southeast Asia, *Theoretical and Applied  
Climatology*, 147, 669–690, <https://doi.org/10.1007/s00704-021-03844-1>, 2022.
- Thrasher, B., Maurer, E. P., McKellar, C., and Duffy, P. B.: Technical Note: Bias correcting climate model simulated daily temperature ex-  
tremes with quantile mapping, *Hydrology and Earth System Sciences*, 16, 3309–3314, <https://doi.org/10.5194/hess-16-3309-2012>, pub-  
lisher: Copernicus GmbH, 2012.
- 755 Thrasher, B., Wang, W., Michaelis, A., and Nemani, R.: NEX-GDDP-CMIP6, <https://doi.org/10.7917/OFSG3345>, 2021.



- Thrasher, B., Wang, W., Michaelis, A., Melton, F., Lee, T., and Nemani, R.: NASA Global Daily Downscaled Projections, CMIP6, Scientific Data, 9, 262, <https://doi.org/10.1038/s41597-022-01393-4>, number: 1 Publisher: Nature Publishing Group, 2022.
- Tian, B. and Dong, X.: The Double-ITCZ Bias in CMIP3, CMIP5, and CMIP6 Models Based on Annual Mean Precipitation, Geophysical Research Letters, 47, e2020GL087232, <https://doi.org/10.1029/2020GL087232>, \_eprint: <https://onlinelibrary.wiley.com/doi/pdf/10.1029/2020GL087232>, 2020.
- 760 Van de Velde, J., Demuzere, M., De Baets, B., and Verhoest, N. E. C.: Impact of bias nonstationarity on the performance of uni- and multivariate bias-adjusting methods, Hydrology and Earth System Sciences Discussions, pp. 1–47, <https://doi.org/10.5194/hess-2020-639>, publisher: Copernicus GmbH, 2020.
- van Hengstum, P. J., Donnelly, J. P., Fall, P. L., Toomey, M. R., Albury, N. A., and Kakuk, B.: The intertropical convergence zone modulates intense hurricane strikes on the western North Atlantic margin, Scientific Reports, 6, 21 728, <https://doi.org/10.1038/srep21728>, number: 1 Publisher: Nature Publishing Group, 2016.
- 765 Warren, R., Hope, C., Gernaat, D. E. H. J., Van Vuuren, D. P., and Jenkins, K.: Global and regional aggregate damages associated with global warming of 1.5 to 4 °C above pre-industrial levels, Climatic Change, 168, 24, <https://doi.org/10.1007/s10584-021-03198-7>, 2021.
- Xu, Z., Han, Y., Tam, C.-Y., Yang, Z.-L., and Fu, C.: Bias-corrected CMIP6 global dataset for dynamical downscaling of the historical and future climate (1979–2100), Scientific Data, 8, 293, <https://doi.org/10.1038/s41597-021-01079-3>, number: 1 Publisher: Nature Publishing Group, 2021.
- 770